

## Next-Generation Improvements in Giant Exoplanet Evolutionary and Structural Models

ANKAN SUR ,<sup>1,2</sup> ROBERTO TEJADA AREVALO ,<sup>1</sup> ADAM BURROWS ,<sup>1</sup> AND YI-XIAN CHEN ,<sup>1</sup>

<sup>1</sup>*Department of Astrophysical Sciences, Princeton University, 4 Ivy Lane, Princeton, NJ 08544, USA*

<sup>2</sup>*Department of Earth, Planetary, and Space Sciences, University of California Los Angeles, 595 Charles E Young Dr E, LA, CA 90095*

### ABSTRACT

We present a comprehensive comparison between legacy and modern evolutionary models for giant exoplanets, using our planetary evolution code, **APPLE**, to emulate and extend previous studies. Our analysis isolates and quantifies the impact of recent physical advances motivated by detailed modeling of Jupiter and Saturn, including updated hydrogen–helium and heavy-element equations of state, helium rain, “fuzzy” cores, and non-adiabatic, inhomogeneous envelopes, alongside improved atmospheric boundary conditions that incorporate ammonia cloud physics. We first examine the influence of each new physical ingredient individually, then construct combined baseline models for masses between 0.3 to 4 Jupiter masses to assess their collective effect on planetary structure and observable properties. We find that the adoption of modern equations of state and realistic heavy-element distributions leads to systematic, but sometimes subtle, differences ( $\sim 5$  to 10%) in radius evolution, while helium rain and the treatment of convection can significantly alter thermal histories and atmospheric compositions (by  $\sim 5$  to 20%). These updated physical processes must be incorporated into the next-generation exoplanet evolutionary models to achieve physically consistent interpretations of planetary observations.

### 1. INTRODUCTION

Structural and evolutionary models of the solar system gas giants Jupiter and Saturn (with masses of 318 and 95 earth masses, respectively) have a long pedigree. Given their masses, it has long been understood that their large radii required hydrogen to be their primary constituent (Demarcus 1958; Peebles 1964; Zapsky & Salpeter 1969; Hubbard 1969; Bodenheimer 1976). Their small inferred thermal conductivities (Hubbard 1966, 1968; Hubbard & Smoluchowski 1973; Stevenson & Salpeter 1977) suggested that convection dominates their energy transport and cooling from birth (Hubbard 1968, 1970; Grossman et al. 1972; Grabske et al. 1975). Their formation out of the protostellar/protoplanetary disk by the assembly of a critical mass heavy-element core (of perhaps  $\sim 10$  earth masses) that nucleated the subsequent rapid accumulation of hydrogen and helium gas to achieve a gas giant had been (and remains, in broad outline) the paradigm for their formation (Mizuno 1980; Stevenson 1982; Bodenheimer & Pollack 1986; Lissauer 1987; Pollack et al. 1996). Hence, what emerged was a model with a fractionally small heavy-element

core surrounded by a convective/adiabatic envelope of predominantly hydrogen and helium (in roughly solar ratios), with a small admixture of heavier elements (in perhaps solar ratios). Convection would homogenize the envelope and make it isentropic. The thin outer atmosphere would act as the valve for energy loss.

This model of a core (that could be thermally inert) with an extensive gas envelope, capped by a molecular atmosphere, has been the conceptual framework for gas giants for decades, epitomized by the pioneering early structural and evolutionary work of Hubbard (Hubbard 1968, 1969, 1970, 1977). After formation, such a model is evolved with an ordinary differential equation for the time derivative of the envelope entropy, an equation of state, and an atmosphere boundary condition (Burrows et al. 1993; Burrows et al. 1995; Guillot et al. 1995; Burrows et al. 1997; Baraffe et al. 1998, 2003; Fortney & Hubbard 2003, 2004; Arras & Bildsten 2006; Fortney et al. 2007; Fortney et al. 2011; Saumon & Marley 2008; Phillips et al. 2020; Marley et al. 2021). An approximation for the thermal effect of solar insolation is attached (whether incorporated into the atmosphere calculation or in an ad hoc fashion), and the time dependence of the planet’s radius, entropy, and luminosity is calculated.

However, recent formation models have suggested the heavy-element core could be extended (Lozovsky et al. 2017; Helled & Stevenson 2017; Stevenson et al.

2022; Bodenheimer et al. 2025) and the gaseous hydrogen/helium envelope could grow coevally with the accumulation of solid planetesimals and/or pebbles. Moreover, recent Juno (Bolton et al. 2017) and Cassini (Spilker 2019; Iess et al. 2019) probe data strongly suggest there are stably-stratified/non-convective regions in both planets and that their envelopes are not homogeneous. They seem to have “fuzzy cores” with extended non-flat distributions of heavy elements (Wahl et al. 2017; Debras & Chabrier 2019; Militzer et al. 2022; Mankovich & Fuller 2021; Howard et al. 2023; Militzer & Hubbard 2024). Given this, the traditional structural and evolutionary models are inadequate, and techniques akin to those employed in stellar evolution are required to model them temporally. This has recently been attempted by our group (Tejada Arevalo et al. 2025; Sur et al. 2024, 2025a,b) and by others (Vazan et al. 2018; Müller et al. 2020; Stevenson et al. 2022).

In light of these developments, a reassessment of literature models for giant exoplanet evolution that adopted the traditional approach employed for solar-system giants would seem in order. Those evolutionary models (Burrows et al. 1995, 1997, 2001; Baraffe et al. 2003; Fortney et al. 2007; Saumon & Marley 2008; Phillips et al. 2020; Marley et al. 2021) have underpinned the global interpretation of observations of giant exoplanets over three decades. However, they generally incorporate the thermally inert core plus fully convective envelope paradigm and use ordinary differential equation solvers for the quasi-hydrostatic evolution of the envelope’s entropy and luminosity. In addition, these exoplanet models do not incorporate helium rain (Burrows et al. 1997; Baraffe et al. 2003; Arras & Bildsten 2006; Fortney et al. 2007; Saumon & Marley 2008; Phillips et al. 2020; Marley et al. 2021) and have generally employed the older equation of state (EOS) (Saumon et al. 1995) for hydrogen/helium mixtures. Finally, they frequently ignored the contribution of the heavy elements to the envelope EOS, ignoring the contribution there of the heavies to the specific heats and the pressures.

With this paper, we set out to explore the differences between heritage giant exoplanet models and those that incorporate updated equations of state, fuzzy core and stably-stratified heavy-element envelopes, helium rain, and updated atmospheric boundary conditions. We here do not set out to provide an extensive grid of such models for general community use. This will follow later. We merely highlight the differences between published models and representative structural and evolutionary models, channeling the more modern perspective (however provisional). To accomplish this, we use the **APPLE** code (Sur et al. 2024). We will see that there can be quantita-

tive differences in the predicted observables, particularly for the lower mass giant exoplanets.

In §2, we describe our choice of hydrogen and helium (H-He) equation of state (EOS), heavy element equation of state, atmosphere boundary conditions, and our handling of heat and composition transport. We reproduce past models with their assumptions and EOSes in §3. We present improved best practices for modeling the evolution of gas giant planets in §4, and compute a sample of new evolution models in §5. We provide concluding remarks in §6.

## 2. METHODS

In the study of giant planets, the H-He EOS plays a central role in the evolution of their effective temperatures, radii, and interior temperature profiles (Militzer & Hubbard 2013; Chabrier et al. 2019). The H-He EOS of Saumon et al. (1995, SCvH95) has been widely used in gas giant planet evolution models, but since such early work did not account for non-ideal entropy and volume interaction terms in the volume-addition law prescriptions (Saumon et al. 1995), it has now been superseded by H-He EOSes that do include such terms (See Tejada Arevalo et al. 2024, and discussions therein). The H-He EOS of Chabrier et al. (2019, CMS19) incorporates these effects in the EOS published by Chabrier & Debras (2021, CD21). The CD21 H-He EOS captures the non-ideal mixing effects of the H-He EOS calculated by Militzer & Hubbard (2013). Most recently, (Howard & Guillot 2023) included these non-ideal effects as a function of helium fraction. The differences between the CD21 EOS and the updates to the CMS19 by Howard & Guillot (2023) are minor, as shown in Figure 4 of Howard & Guillot (2023) and Figure 1 of Tejada Arevalo et al. (2024). We further note here that recent experimental results by Liu et al. (2025) show good agreement with both the CD21 EOS and the Howard & Guillot (2023) results. We therefore use the updated H-He EOS of CD21 in later sections to remain consistent with our previous work (e.g., Tejada Arevalo et al. 2025; Sur et al. 2025a).

The metal ( $Z$ ) EOS is here represented by the multi-phase water calculations of Haldemann et al. (2020, AQUA), which includes the calculations of Mazeved et al. (2019).<sup>1</sup> Throughout this work, the solar metallic-

<sup>1</sup> As Aguichine et al. (2025) pointed out, the water EOS of Mazeved et al. (2019) contained an error in the non-ideal entropy terms which did not affect the density. This has then been corrected (Mazeved et al. 2021), but no other comprehensive water EOS tables are currently available. Our own calculations and those of Tejada Arevalo (2025) suggest that these corrections are small and inconsequential to any conclusions in this work.

ity ( $1 Z_{\odot}$ ) is taken to be 0.0156 by mass. We distinguish between *metallicity* and *metal fraction* where metallicity is quoted as a ratio to solar values, and metal fractions are always metal mass fractions.<sup>2</sup>

Heat and composition transport is primarily treated via mixing-length-theory convection under the Ledoux criterion (Ledoux 1947). Any region which meets the Ledoux criterion is convective, and regions which do not meet this criterion are stable to convection. In stable regions, conduction and microscopic diffusion are assumed to be the dominant modes of heat and composition transport. Our evolution code **APPLE** and its heat and composition transport methodology is fully described in Sur et al. (2024). Moreover, a comprehensive discussion on our applications of the Ledoux criterion is found in Section 2 of Tejada Arevalo et al. (2025). In §5, we discuss the implications of using the Schwarzschild criterion (Schwarzschild & Häm 1965).

The effects of semiconvection, or “double-diffusive” convection, are omitted in this study due to the existing uncertainties in its treatment and in the relevant microphysical properties. While semiconvection could affect the evolution of helium rain layers and stably-stratified regions in gas giant fuzzy cores, their impact on 1-D evolution models may be minor (See Figure 8 of Müller et al. 2020), though this is still an open question.

### 3. REPRODUCTION OF PAST EVOLUTIONARY MODELS

Most evolutionary calculations in the past assumed adiabatic interiors, omitted solid cores, neglected rotation, and did not account for the effects of helium rain. Here, we reproduce a series of exoplanet evolutionary histories from various groups using the planetary evolution code **APPLE** (Sur et al. 2024), adopting their same assumptions, for a range of planetary masses spanning from Saturn mass up to a few Jupiter masses as shown by the colored lines in Figure 1. This exercise is conducted to ensure we can emulate past models and practices. The top-left panel presents the evolutionary sequences from Burrows et al. (1997), where the envelope helium mass fraction is  $Y = 0.25$  and the interior is modeled using the SCvH95 equation of state (Saumon et al. 1995). Atmospheric boundary conditions are provided by the isolated, non-gray model atmosphere grids of Burrows et al. (1997). Their study modeled solar-metallicity objects spanning  $0.3 M_{\text{Jup}}$  to  $70 M_{\text{Jup}}$  (down to  $T_{\text{eff}} \sim 100$  K) using a sophisticated at-

mospheric boundary condition that employed a detailed molecular opacity and equilibrium database. The top-right panel displays the reproduction of evolutionary sequences based on the irradiated atmospheric boundary tables of Fortney et al. (2011) for Jupiter- and Saturn-mass planets, assuming a metallicity of 3.16 times the solar value and adopting the SCvH95 EOS for the hydrogen–helium mixture. In these models, the Jupiter case includes a  $10 M_{\oplus}$  core composed of iron and post-perovskite, with an envelope heavy-element mass fraction  $Z = 0.059$  and employing the old AQUA EOS, while the Saturn case assumes a  $21 M_{\oplus}$  core with a  $Z = 0.03$  envelope. The bottom-left panel presents the reproduction of models from Phillips et al. (2020), which extend the earlier work of Baraffe et al. (2003). In our implementation within **APPLE**, the ATMO atmospheric grids from Phillips et al. (2020) are combined with the CMS19 H–He EOS (Chabrier et al. 2019) for the envelope. Rather than using a dedicated heavy-element EOS, these models mimic the effect of heavy elements by adopting an effective helium fraction,  $Y' = Y + Z = 0.2919$ , which increases the mean molecular weight of the mixture. Finally, the bottom-right panel shows our reproduction of models from the Sonora Bobcat suite (Marley et al. 2021) with  $[\text{M}/\text{H}] = -0.5$  (corresponding to  $Z = 0.00484$ ) using their boundary conditions<sup>3</sup>. The Sonora Bobcat grid solved the coupled atmosphere–interior structure equations over  $T_{\text{eff}} = 200$ – $2400$  K and  $\log g = 3$ – $5.5$ , incorporating updated opacities, rainout chemistry, and the SCvH95 EOS with metals. Similar to Phillips et al. (2020) models, the effect of heavy elements in the Sonora models is also not captured through a separate EOS, but is instead mimicked by adopting an effective helium fraction  $Y' = Y + Z = 0.27834$  (where  $Y = 0.2735$ ). We thus demonstrate that, under the different model assumptions described above, **APPLE** can successfully reproduce and emulate previous evolutionary calculations.

### 4. IMPROVEMENTS IN GIANT EXOPLANETS MODELING

Having reproduced the heritage evolutionary models using **APPLE**, we present in this section the individual effects of new aspects that have emerged subsequently in giant planet models and modeling. These include using realistic heavy-element equations of state instead of an augmented helium fraction, improvements in the overall

<sup>2</sup> For example, 10, 100, and 1000  $Z_{\odot}$  metallicities are 0.136, 0.613, and 0.941 metal fraction by mass, respectively, assuming  $1 Z_{\odot} = 0.0156$ .

<sup>3</sup> The Sonora Bobcat boundary tables extend down to  $T_{\text{eff}} = 200$  K. In this study, we extrapolated the tables below this limit, as did Marley et al. (2021) for the original Sonora models (Mark Marley & Didier Saumon, private communication)

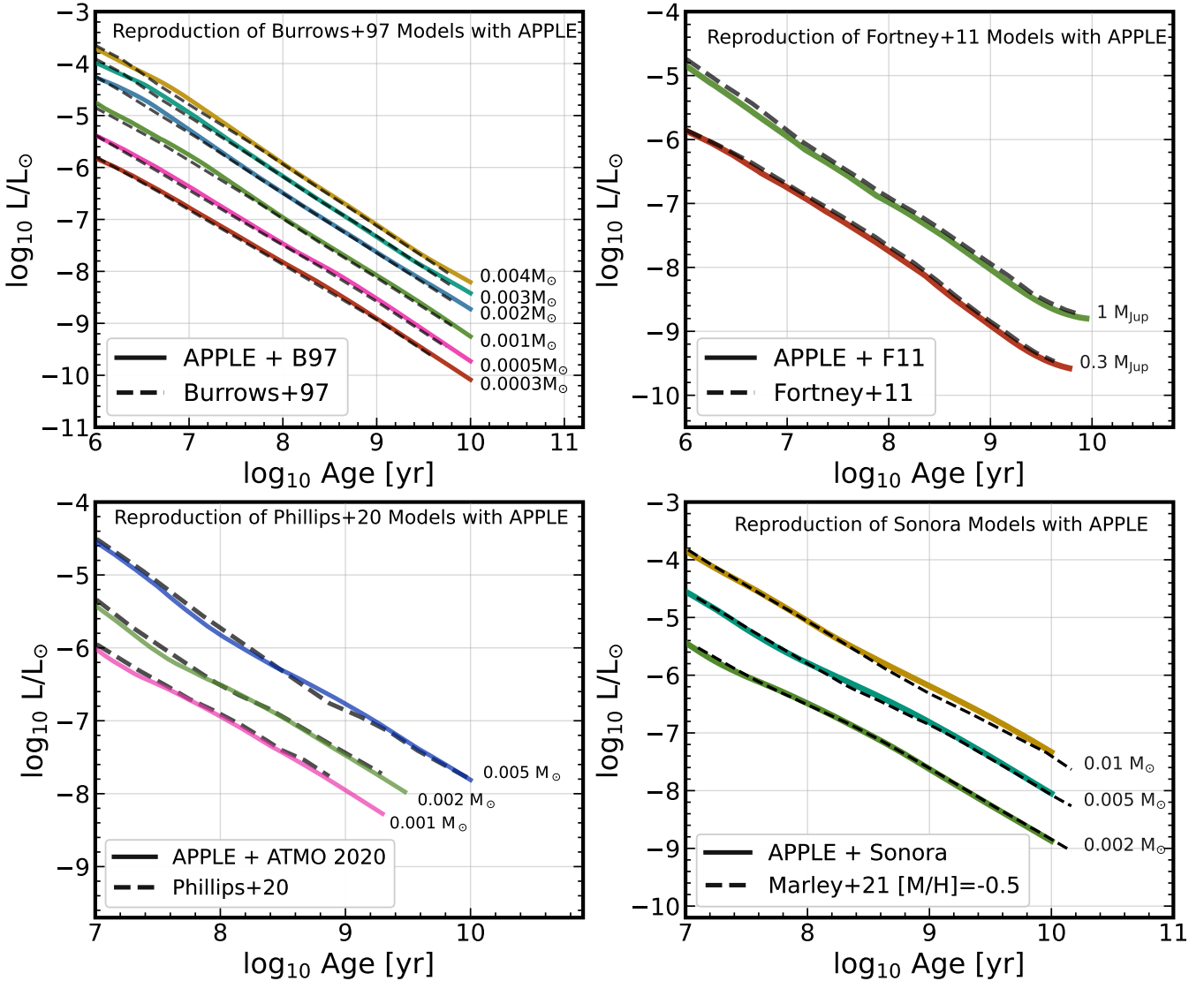


**Figure 1.** Reproduction of various heritage exoplanet evolutionary models (dashed black curves) using the model setups and inputs in those papers, as computed with **APPLE** (Sur et al. 2024) (solid colored lines) for a range of planetary masses. Masses are indicated next to each line (in units of solar masses) and luminosities are in solar units. Unless explicitly stated otherwise, all models are adiabatic, have no solid core, neglect rotation, and neglect helium rain. Top left: Evolutionary sequences from Burrows et al. (1997). The envelope helium mass fraction is  $Y = 0.25$ , and the interior is modeled with the SCvH95 equation of state (Saumon et al. 1995). Atmospheric boundary conditions are taken from the isolated, non-gray model atmosphere grids of Burrows et al. (1997). Top right: Evolutionary sequences computed using the irradiated atmospheric boundary tables of Fortney et al. (2011) for Jupiter- and Saturn-mass planets, assuming  $3.16 Z_{\odot}$  metallicity and the SCvH95 EOS for hydrogen-helium mixture. The Jupiter model includes a  $10 M_{\oplus}$  core composed of iron and post-perovskite, with an envelope heavy-element mass fraction  $Z = 0.059$  and using the AQUA EOS (Haldemann et al. 2020). The Saturn model assumes a  $21 M_{\oplus}$  core with an envelope  $Z = 0.03$ . Bottom left: Models from Phillips et al. (2020), which extend the earlier Baraffe et al. (2003) evolutionary calculations. In **APPLE**, we implement the ATMO atmospheric grids from Phillips et al. (2020) together with the CMS19 H-He EOS (Chabrier et al. 2019), adopting as they did an effective helium fraction  $Y' = Y + Z = 0.2919$  to approximate a mixture of helium and heavy elements. No dedicated heavy-element EOS is employed in these models. Bottom right: Models from the Sonora-Bobcat suite (Marley et al. 2021) with  $[M/H] = -0.5$  (corresponding to  $Z = 0.00484$ ), which also treat the interior with the SCvH95 H-He EOS, using an effective  $Y' = Y + Z = 0.27834$  (with  $Y = 0.2735$ ) to approximate the contribution of heavy elements (as did they) and their published atmosphere boundary conditions.

equation of state of hydrogen/helium mixtures, updates to the atmosphere boundary conditions, the effects of helium rain, the effect of the possible presence of an extended fuzzy core of heavy elements, and an example of the potential effects of the initial thermal profiles on the subsequent evolution.

#### 4.1. Treatment of Heavy Elements in Giant Exoplanet Evolution Models

In earlier evolutionary models, heavy elements were often not treated with a dedicated equation of state. Instead, their contribution was approximated by folding them into an effective helium mass fraction,  $Y' = Y + Z$ , as in Chabrier & Baraffe (1997); Chabrier (2003); Saumon & Marley (2008); Phillips et al. (2020); Marley et al. (2021). This approach provided a computationally simpler alternative, but neglected the distinct thermodynamic behavior of heavy elements/“metals”. To assess the impact of this approximation on the adiabatic evolution of giant planets, we compare such models to those in which envelope heavy elements are treated explicitly using the AQUA EOS (Haldemann et al. 2020).

The resulting evolutionary tracks are shown in Figure 2 for masses ranging from 0.3 to  $4 M_{\text{Jup}}$ . All calculations employ the Sonora Bobcat atmospheric boundary conditions with an envelope metallicity of  $3.16 Z_{\odot}$  (Marley et al. 2021), a fixed helium mass fraction  $Y = 0.2735$  treated with the SCvH95 EOS, and assume coreless, non-rotating planets. Solid lines represent models that employ the AQUA EOS, while the dashed curves specifically correspond to Sonora models that approximate heavy elements with an effective helium fraction of  $Y' = 0.3219$ . In the top panel, we compare the effective temperatures and planetary radii, while in the bottom panel, we show the temperature profiles at 1 and 5 Gyr, respectively, highlighting the differences that arise in the planetary interiors due to the different EOS treatments.

Quantitatively, the two approaches yield similar evolutionary tracks, with median relative differences of only  $\sim 0.6$  to  $0.75\%$  in effective temperature and  $\sim 0.3$  to  $0.5\%$  in planetary radii. However, the internal temperature profiles show somewhat larger discrepancies, on the order of 4.5 to 7%, underscoring the importance of an explicit EOS treatment when precise thermal structures are required.

#### 4.2. Impact of Metal Distribution on Evolutionary Properties

We next examine how the spatial distribution of heavy elements influences the evolution of giant planets. Two limiting configurations are considered: in the first, heavy elements are assumed to be homogeneously

mixed throughout the entire envelope, with no distinct compact core. In the second, the same heavy-element mass is concentrated entirely into a central core, leaving a metal-free envelope. In all cases, the total heavy-element mass fraction is fixed at  $Z = 0.0484$  ( $3.16 Z_{\odot}$ ), which corresponds to heavy-element masses of approximately 4.61, 15.38, 30.76, and  $61.52 M_{\oplus}$  for planets of 0.3, 1, 2, and  $4 M_{\text{Jup}}$ , respectively.

All evolutionary calculations employ the Sonora Bobcat atmospheric boundary conditions with  $Z = 0.0484$  (Marley et al. 2021). The hydrogen–helium component of the envelope is treated with the SCvH95 EOS for a fixed helium fraction  $Y = 0.2735$ , while the heavy elements are represented using the AQUA EOS (Haldemann et al. 2020), both in the envelope and in the core. This consistent treatment allows for a controlled comparison between the two distributional exemplars.

The results are shown in Figure 3 for both the time evolution of the effective temperature and planetary radius, and the relative differences between the two cases. While the global properties remain broadly similar, the models reveal systematic differences: planets with metals distributed throughout the envelope are systematically smaller than planets with metals concentrated in the core. The radius differences are on the order of  $\sim 1.0$ – $1.3\%$  across all masses and evolutionary times, while effective temperatures vary by only  $\sim 0.7$ – $1\%$ . These results suggest that even in adiabatic models, the distribution of heavy elements can introduce measurable shifts, complementing the more commonly examined dependence on total heavy-element content.

#### 4.3. Comparison of Hydrogen–Helium Equations of State

All heritage exoplanet models, such as Burrows et al. (1997); Chabrier & Baraffe (1997); Baraffe et al. (1998, 2003); Fortney & Hubbard (2004); Saumon & Marley (2008); Marley et al. (2021), used the SCvH95 (Saumon et al. 1995) EOS tables for modeling hydrogen and helium. To quantify the influence of hydrogen–helium thermodynamics on planetary evolution, we compare the older SCvH95 model to the more recent CD21 tables (Chabrier & Debras 2021). These EOSs differ in their treatment of non-ideal effects and phase transitions, and thus provide a useful test of how updates in microphysics translate into macroscopic observables of giant planets.

We evaluate the models under the Sonora Bobcat (Marley et al. 2021) atmospheric boundary conditions as implemented within the `APPLE` code. The left panel presents the evolution of effective temperatures, while the right panel shows the evolution of planetary radii for masses ranging from 0.3 to  $4 M_{\text{Jup}}$ . The models

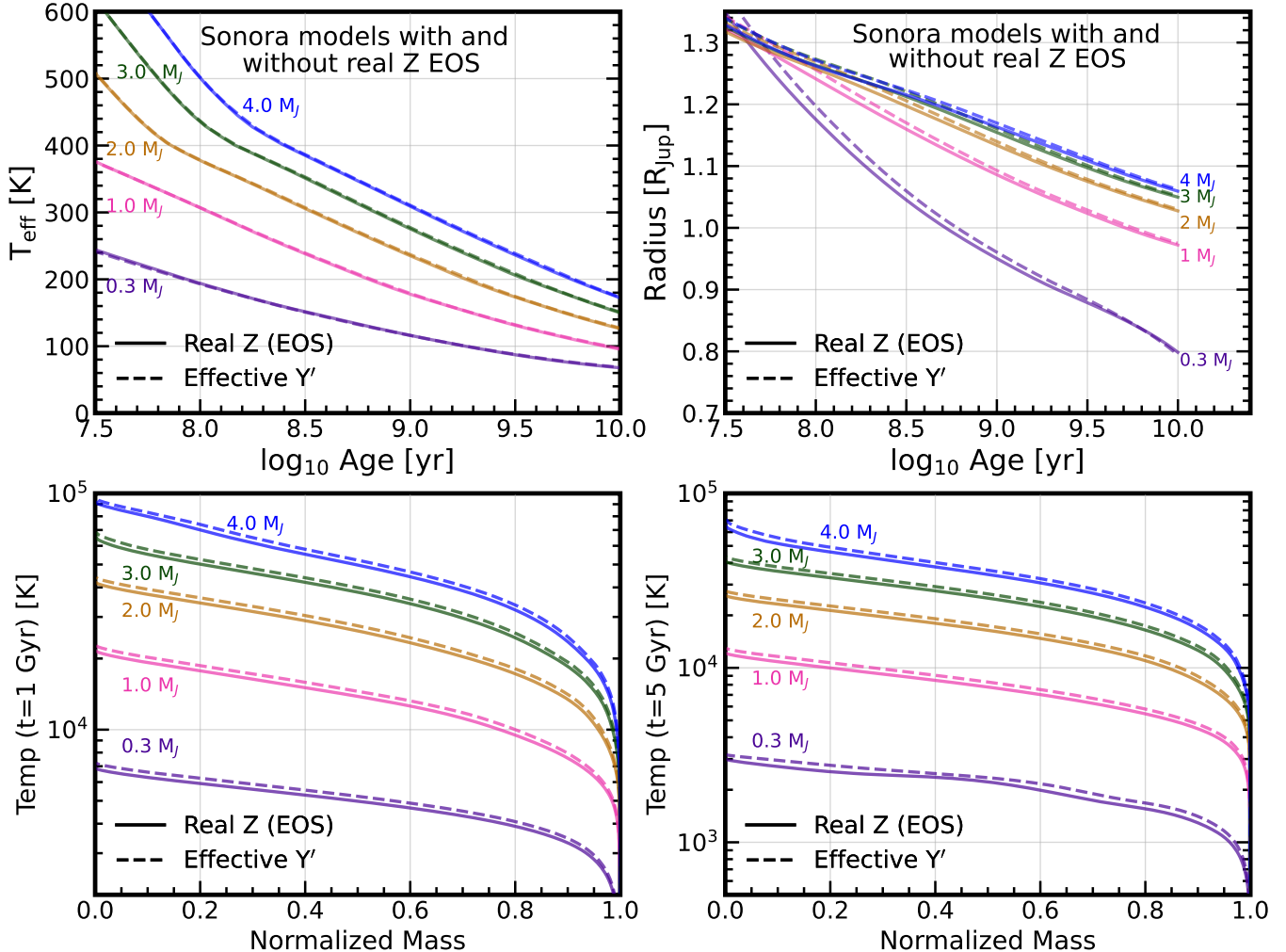


**Figure 2.** Comparison of adiabatic evolution models of giant planets with different treatments of heavy elements: solid lines correspond to models where heavy elements in the envelope are treated with the AQUA EOS (Haldemann et al. 2020), while dashed lines represent models in which the effect of heavy elements is not modeled with a dedicated  $Z$  EOS, but is instead approximated by an effective helium fraction  $Y' = Y + Z = 0.27834$  (as has traditionally been done). The top panel shows the evolution of the effective temperatures and radii, while the bottom panel shows the temperature profiles at 1 and 5 Gyr, respectively. All calculations use the Sonora Bobcat atmospheric boundary conditions (Marley et al. 2021) with  $[M/H] = +0.5$ , and cover planetary masses ranging from 0.3 to  $4 M_{\text{Jup}}$ . The helium mass fraction in the envelope is fixed at  $Y = 0.3219$ , treated with the SCvH95 EOS. All models assume coreless, non-rotating planets. For the various masses, the median relative errors range from  $\sim 0.6\%$  to  $0.75\%$  for  $T_{\text{eff}}$ ,  $\sim 0.3\%$  to  $0.5\%$  for the radii, and  $\sim 4.5$  to  $7\%$  for the temperature profiles.

are isolated and coreless, with an envelope metallicity of  $Z=0.00484$  and helium mass fraction  $Y = 0.2735$ . In these models, heavy elements are not treated with a dedicated EOS, but are instead folded into an effective helium fraction,  $Y' = Y + Z = 0.27834$ , following the prescription of Marley et al. (2021).

The quantitative differences between SCvH95 and CD21 shown in Figure 4 depend primarily on planetary mass. For effective temperatures, the relative differences between the two EOSs remain modest, ranging from  $\sim 1.9\%$  for the  $0.3 M_{\text{Jup}}$  case to  $\sim 0.6\%$  for the  $4 M_{\text{Jup}}$  case. The impact on planetary radii, however, is

more pronounced. Over 10 Gyr, the radius differences increase from  $\sim 0.6\%$  at higher masses to as much as  $\sim 6.7\%$  at lower masses. These results indicate that while updates to the hydrogen–helium EOS have only a limited effect on the thermal evolution of more massive giant planets, they can lead to significant structural differences for lower-mass giants. Similar conclusions were reached by Chabrier & Debras (2021) and Howard et al. (2025), the latter comparing results of the Chabrier et al. (2019) H-He EOS with the Howard & Guillot (2023) corrections to the SCvH95 EOS on giant exoplanet interiors. Further, it has also been shown that the difference

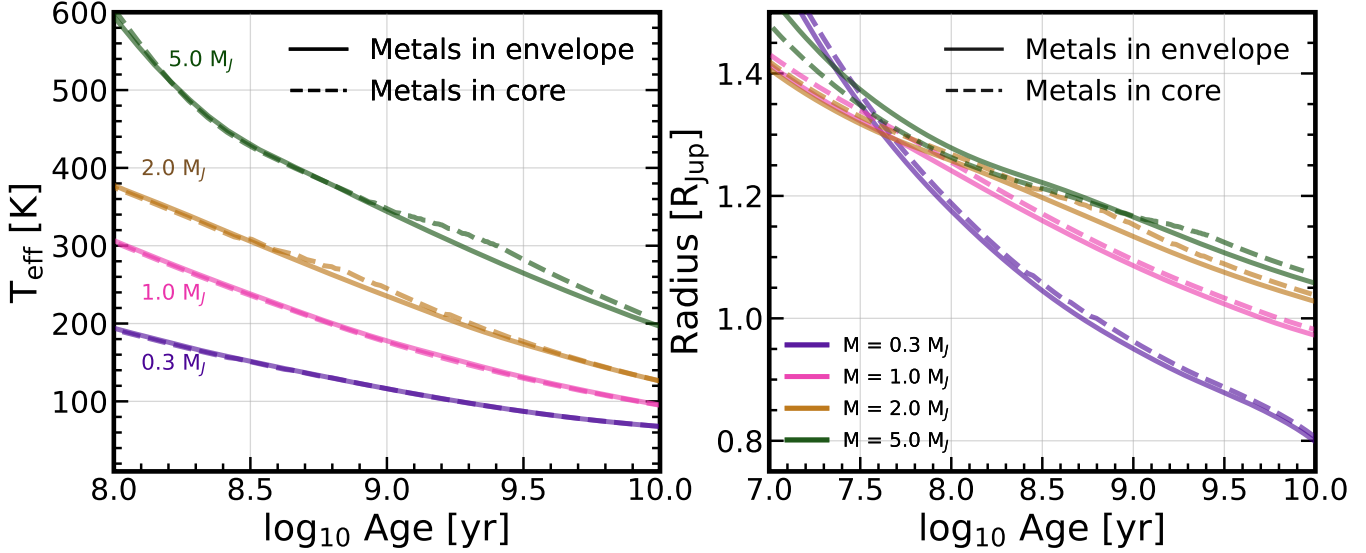


**Figure 3.** Evolution of giant planets comparing models where (i) metals are uniformly mixed throughout the envelope without a compact core and (ii) all metals are concentrated entirely in the core. The bulk metallicity for all the models is  $3.16 Z_{\odot}$  ( $Z = 0.0484$ ). This corresponds to  $4.61, 15.38, 30.76, 76.9 M_{\oplus}$  for the  $0.3, 1, 2$ , and  $5 M_{J_{\text{up}}}$  models, respectively. All calculations adopt the Sonora Bobcat atmospheric boundary conditions (Marley et al. 2021). The helium mass fraction in the envelope is fixed at  $Y = 0.2735$  and treated with the SCvH95 EOS, while heavy elements are represented by the AQUA EOS in both the core and the envelope. Assuming that the same heavy elements reside in the core versus in the envelope results in a difference of  $\sim 0.9$  to  $1.3\%$  in the radius for all times. This suggests that, contrary to the common simplifying assumption of radius being independent of the heavy-element distribution at fixed mass fraction, modest but systematic differences can arise even in adiabatic models. The median relative errors for  $T_{\text{eff}}$  range from  $0.12\%$  for  $0.3 M_{J_{\text{up}}}$  to  $5\%$  for  $5 M_{J_{\text{up}}}$  over 5 Gyr.

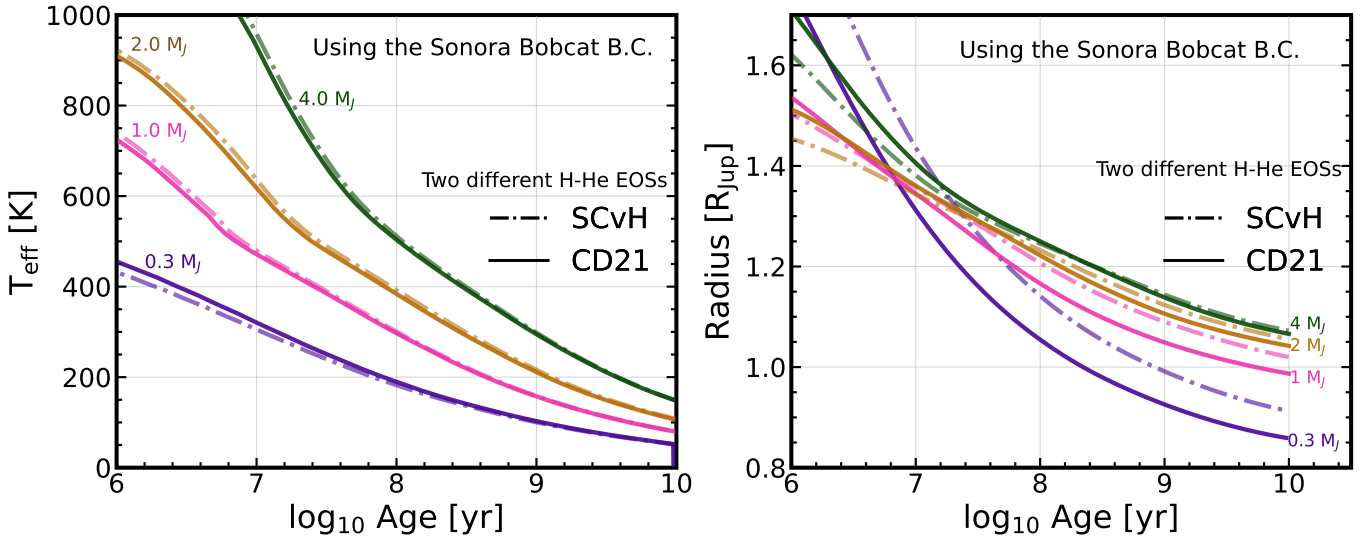


**Figure 4.** Adiabatic evolution of giant planets, comparing two hydrogen–helium equations of state: the old SCvH95 (Saumon et al. 1995, dot-dashed lines) and the latest CD21 (Chabrier & Debras 2021, solid lines) using atmospheric boundary conditions from the Sonora Bobcat grids. The left panel shows the evolution of effective temperature, while the right panel shows the evolution of planetary radius, for masses ranging from  $0.3$  to  $4 M_{J_{\text{up}}}$ . All models are isolated, nonrotating, and coreless, with an envelope metallicity of  $[\text{M}/\text{H}] = -0.5$  ( $Z = 0.00484$ ) and a helium mass fraction fixed at  $Y = 0.2735$ . The contribution of heavy elements is not modeled with a dedicated EOS, but is instead approximated by adopting an effective helium fraction  $Y' = Y + Z = 0.27834$ , following the approach of Marley et al. (2021). The median relative errors over 10 Gyr between the two EOSs for  $T_{\text{eff}}$  range from  $1.9\%$  for  $0.3 M_{J_{\text{up}}}$  to  $0.6\%$  for  $4 M_{J_{\text{up}}}$ . The effect of the modern EOS on radius is more pronounced, increasing from  $\sim 0.6\%$  at higher masses to  $\sim 6.7\%$  at lower masses.

in H-He EOS for Jupiter and Saturn has consequences for superadiabaticity (Howard et al. 2024), and the total metal content required to fit the Juno data (Miguel et al. 2016).

#### 4.4. Sensitivity to Atmospheric Boundary Conditions

We also investigate how the choice of atmospheric boundary conditions influences the adiabatic evolution of giant planets. Two widely used boundary models: the grids of the Sonora Bobcat models of Marley et al. (2021), and the earlier tables of Burrows et al. (1997), are compared with the more recent Chen et al. (2023) boundary condition. The latter was originally developed to model Jupiter and Saturn (Tejada Arevalo et al. 2024; Sur et al. 2025a,b) and included irradiation, but we have expanded our isolated boundary tables to cover the giant exoplanet parameter space. At the lowest effective temperatures, the Chen et al. (2023) boundary conditions also include the effects of ammonia cloud formation. Hence, these various outer thermal boundary models represent different generations of atmosphere calculations, incorporating advances in opacities, radiative transfer, and molecular chemistry, and thus provide a benchmark for the robustness of planetary cooling models to outer boundary assumptions.

Our calculations span planetary masses from 0.3 to  $4 M_{\text{Jup}}$ . All models shown in this section assume coreless planets with fully adiabatic, homogeneous hydrogen–helium envelopes with envelope metallicity of  $3.16 Z_{\odot}$ . The helium mass fraction is fixed at  $Y = 0.2735$ , treated with the SCvH95 EOS, while heavy elements are modeled as ices using the AQUA EOS. This setup isolates the effect of the atmosphere tables by keeping the interior physics fixed.

The results shown in Figure 5 reveal that boundary conditions play a non-negligible role in shaping the thermal evolution. At late times, effective temperatures differ by  $\sim 7\%$  for the  $0.3 M_{\text{Jup}}$  case, while the discrepancy decreases to  $\sim 3\%$  for the  $4 M_{\text{Jup}}$  planet. The corresponding planetary radii at a given age differ by about 3–6% across the mass range. Early in the evolution, however, the spread among models is much larger, reflecting both the stronger influence of boundary conditions at high entropies and the critical uncertainty in the initial thermal profiles inherited from formation.

Overall, these comparisons demonstrate that atmospheric boundary conditions introduce systematic uncertainties in both  $T_{\text{eff}}$  and planetary radii, especially at young ages, and highlight the importance of using updated atmosphere models in conjunction with consistent initial conditions.

#### 4.5. Effects of Helium Rain on Giant Exoplanet Evolution

Helium rain has long been recognized as a key process in the evolution of solar system giant planets, invoked originally to explain the depleted atmospheric helium abundance in Jupiter and to account for the anomalous luminosity of Saturn (Stevenson & Salpeter 1977; Fortney & Hubbard 2003; Mankovich et al. 2016; Püstow et al. 2016; Mankovich & Fortney 2020; Howard et al. 2024; Tejada Arevalo et al. 2025; Sur et al. 2025a). To date, the only study that has explicitly considered helium rain in the context of exoplanets is Fortney & Hubbard (2004). Given its demonstrated importance for the solar system giants, incorporating helium rain should be a priority for the next generation of exoplanet evolutionary models, particularly at the lowest masses.

To explore the role of helium phase separation, we compare evolutionary models with and without helium rain for planets of 1, 2, and  $3 M_{\text{Jup}}$ . The baseline reference is given by homogeneous, fully adiabatic Sonora Bobcat models, against which we contrast helium-rain models calculated with the diffusion scheme B implemented in APPLE (Sur et al. 2024). Convective stability is assessed using both the Ledoux and Schwarzschild criteria, as shown by the solid and dashed curves, respectively, in Figure 6.

All models adopt the Sonora Bobcat atmospheric boundary conditions at  $3.16 Z_{\odot}$  metallicity. Hydrogen–helium mixtures are described with the SCvH95 EOS, while helium immiscibility is governed by the phase diagram of Lorenzen et al. (2009, 2011, L0911), shifted upward by  $+300$  K. This calibration was previously demonstrated to reproduce both Jupiter’s and Saturn’s effective temperatures and atmospheric helium abundances (Tejada Arevalo et al. 2024; Sur et al. 2025b), and we therefore apply the same shift here. Neither rotation nor the presence of a dense core is considered in this set of calculations.

The results highlight moderate, but systematic, differences between homogeneous and helium-rain cases for the Sonora Bobcat models. At 5 Gyr, the effective temperatures of helium-rain models differ from homogeneous models by approximately  $-20$  K to  $-60$  K under Ledoux convection, and by  $+25$  to  $+5$  K under Schwarzschild convection, from lower- to higher-mass planets, respectively. This contrast has not been explored previously by Fortney & Hubbard (2004), who considered only Schwarzschild convection and, therefore, found only a rise in effective temperature during evolution. The median relative error in planetary radius at this age is  $\sim 1\%$  to  $3\%$  for both convection criteria. The atmospheric helium fraction in the Ledoux models

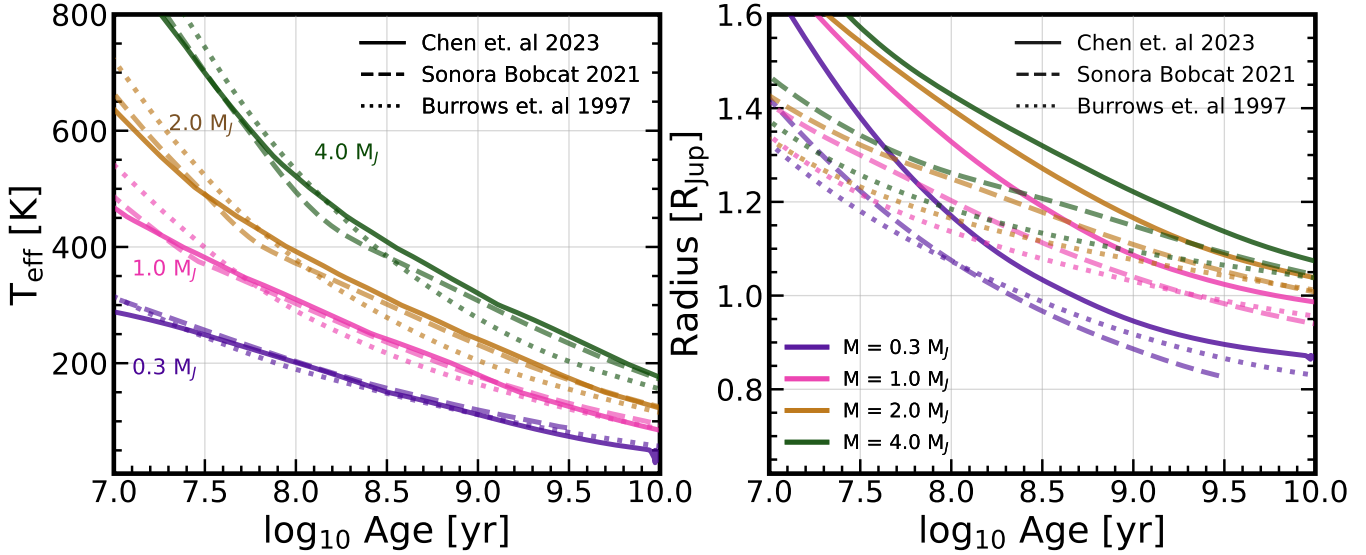


**Figure 5.** Adiabatic evolution of giant planets comparing three atmospheric boundary conditions: Chen et al. (2023, solid lines), Marley et al. (2021, Sonora-Bobcat, dashed lines), and Burrows et al. (1997, dotted lines). Models are shown for planetary masses ranging from 0.3 to  $4 M_{\text{Jup}}$ . All calculations assume coreless planets with homogeneous and adiabatic hydrogen–helium envelopes mixed with heavy-element ices, treated using the AQUA EOS. The helium mass fraction in the envelope is fixed at  $Y = 0.2735$ , modeled using the CD21 EOS, and an atmospheric metallicity of  $3.16 Z_{\odot}$  is adopted and taken as homogeneous throughout the structure for all models. At late times, the effective temperature differences among the various atmospheric boundary conditions range from about 7% for lower-mass planets to  $\sim 3\%$  for higher-mass cases. The corresponding radii differ by approximately 3 to 6% at late times, while at early times the discrepancies can be significantly larger. Note that at early times, the issue of the proper initial thermal profiles inherited from the formation is of primary relevance.

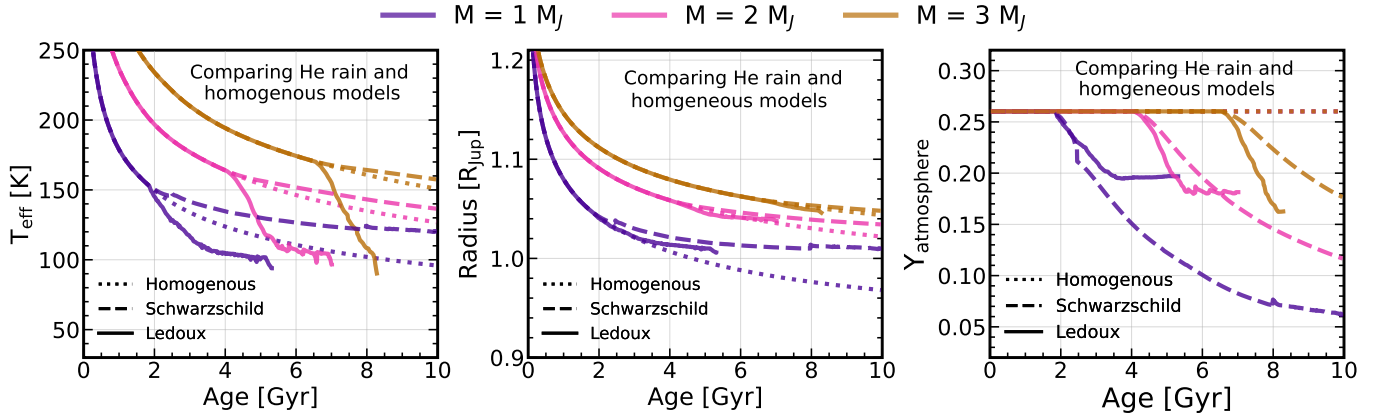


**Figure 6.** Evolution of giant planets comparing helium-rain models with homogeneous adiabatic Sonora Bobcat models without it for 1, 2, and  $3 M_{\text{Jup}}$  planets. Solid curves indicate convective stability using the Ledoux criterion, while dashed curves correspond to the Schwarzschild criterion. All models employ the Sonora Bobcat atmospheric boundary conditions with  $3.16 Z_{\odot}$  metallicity, and a helium fraction of  $Y = 0.2735$  in the envelope is treated with the SCvH95 EOS. The hydrogen–helium miscibility curve of Lorenzen et al. (2009, 2011, L0911), shifted by  $+300$  K, is adopted in this study. This specific shift was previously shown to provide a simultaneous fit to both Jupiter and Saturn (Sur et al. 2025b), successfully matching their effective temperatures and atmospheric helium abundances, and we therefore use the same calibration here. Rotation and the presence of a core are not considered here. At 5 Gyr, helium-rain models differ from homogeneous cases by  $-20$  to  $-60$  K in  $T_{\text{eff}}$  under Ledoux convection and by  $+25$  to  $+5$  K under Schwarzschild convection, with radius offsets of only  $\sim 1$  to 3%. Atmospheric helium is moderately depleted in Ledoux models ( $Y_{\text{atm}} \sim 0.16$  to 0.20) but strongly depleted in Schwarzschild models ( $Y_{\text{atm}} \sim 0.06$  by 10 Gyr). The  $3 M_{\text{Jup}}$  planet undergoes helium rain after only 6 Gyr, indicating a diminishing role at higher masses. These models omit fuzzy cores and metal gradients, and thus differ significantly from our previously published Jupiter models (Tejada Arevalo et al. 2025; Sur et al. 2025a,b).

spans  $Y_{\text{atm}} \sim 0.16$  to 0.20, whereas the Schwarzschild models exhibit much stronger depletion, reaching as low as  $Y_{\text{atm}} \sim 0.06$  at 10 Gyr. Note that the  $3 M_{\text{Jup}}$  planet undergoes helium rain only at much later times ( $> 6$  Gyr) and remains nearly adiabatic, indicating that helium rain plays a diminishing role in more massive exoplanets. These calculations do not attempt to fit Jupiter and exclude both fuzzy cores and inhomogeneous metal distributions, and therefore yield different atmospheric helium abundances than our previous predictions (Sur et al. 2025a,b). We further note that the Ledoux models become noisy at low temperatures ( $\sim 100$  K), where the  $T_{\text{eff}}$  are significantly extrapolated beyond the Sonora Bobcat boundary condition tables<sup>4</sup>. Overall, we conclude that helium rain plays a significant role in the early evolutionary stages of lower-mass gas giants, altering their cooling rates, but its influence diminishes progressively for planets more massive than  $\sim 3 M_{\text{Jup}}$  at Solar System ages.

#### 4.6. Influence of Fuzzy Cores on Giant Exoplanet Evolution

Results from Juno (Bolton et al. 2017) and Cassini (Iess et al. 2019) have fundamentally reshaped interior models of the solar system’s giant planets, favoring the presence of “fuzzy” cores (Wahl et al. 2017; Militzer et al. 2022; Militzer & Hubbard 2024; Mankovich & Fuller 2021) over traditional compact ones. Such fuzzy cores have already been incorporated into evolutionary models of Jupiter and Saturn (Tejada Arevalo et al. 2025; Sur et al. 2025a,b), but they have not yet been systematically explored in the context of exoplanets. An important open question concerns both the initial extent of the fuzzy core and its long-term survival over Gyr timescales, since convective mixing is expected to gradually erode compositional gradients (Knierim & Helled 2024; Tejada Arevalo et al. 2025; Fuentes & Cumming 2021; Fuentes et al. 2025), potentially leading to full homogenization. This not only has observational consequences for their atmospheric metallicity (Knierim & Helled 2025), but also for the origin of close-in giant planets (Knierim et al. 2022).

We investigate the evolutionary consequences of different initial fuzzy-core extents by comparing models of a  $2 M_{\text{Jup}}$  exoplanet with three distinct degrees of fuzzy core extent: mild, moderate, and extended. All fuzzy-core models are constructed using the AQUA EOS for heavy elements, with hydrogen–helium mixtures treated using the CD21 EOS. The helium mass fraction is fixed at  $Y = 0.2735$ , and the models employ Sonora Bobcat

atmospheric boundary conditions at  $3.16 Z_{\odot}$ . The comparison also includes a homogeneous adiabatic reference model, in which the envelope metallicity is  $Z = 0.236$ . All models have a total heavy element mass of  $150 M_{\odot}$ . This is chosen as an example to illustrate the models’ ability to undergo substantial mixing, allowing us to quantify the differences between various observables in this context. Rotation and helium rain are neglected here to isolate the role of fuzzy cores.

The evolutionary tracks are shown in terms of both internal and global properties. The top panels of Figure 7 illustrate the evolution of temperature, entropy, and heavy-element fraction profiles at three characteristic ages: 0.001 Gyr, 0.5 Gyr, and 5 Gyr. The bottom panels present the corresponding time evolution of effective temperature, planetary radius, and atmospheric metallicity. The results demonstrate that the extent of the initial fuzzy core strongly influences the efficiency and timescale of compositional mixing. The extended fuzzy core rapidly homogenizes with the envelope ( $\leq 0.01$  Gyr), followed by the moderately fuzzy core ( $\sim 1$  Gyr), while the mildly fuzzy core remains largely intact and persists beyond 10 Gyr. The extent of mixing is, however, dependent on the chosen initial entropy profiles, as hotter entropies will lead to rapid homogenization of the fuzzy cores (Knierim & Helled 2024; Tejada Arevalo et al. 2025).

Quantitatively, the fuzzy-core models differ appreciably from the homogeneous case. The median relative deviations range from 8%–12% for effective temperature and 8%–13% for planetary radius, indicating that observable properties retain a measurable memory of the planet’s initial compositional structure. The atmospheric metallicity also evolves in a manner correlated with the degree of initial “fuzziness”, increasing from  $Z \simeq 0.02$  in the mild fuzzy case to  $Z \simeq 0.25$  in the extended and moderate fuzzy cases. These results highlight the importance of fuzzy-core physics (Fuentes et al. 2025) in shaping both the long-term cooling and the observable atmospheric properties of giant exoplanets.

#### 4.7. Influence of Initial Conditions on the Fuzzy-Cores of Giant Exoplanet Evolution

Here, we examine how different initial thermal states affect the long-term evolution of a  $2 M_{\text{Jup}}$  planet by comparing three models: a hot-start fuzzy-core case, a cold-start fuzzy-core case, and a homogeneous Sonora Bobcat model. The fuzzy-core models begin with extended regions of heavy elements, while the homogeneous model is coreless and assumes a uniform envelope metallicity of  $Z = 0.236$ . The total heavy element mass in all our models is  $150 M_{\oplus}$ . All calculations employ the Sonora

<sup>4</sup> private communication: Mark Marley & Didier Saumon

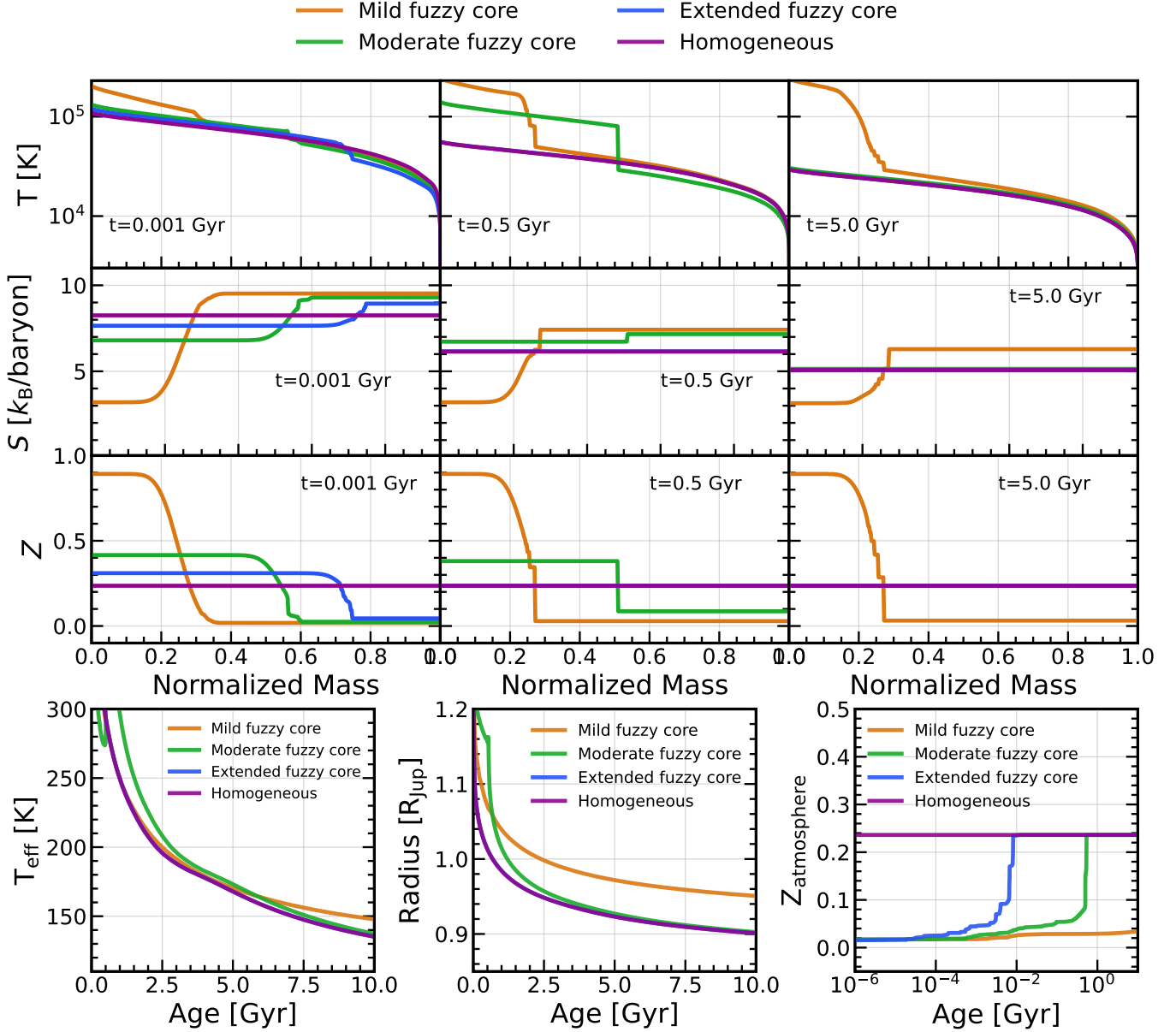


**Figure 7.** Comparison of the evolution of a  $2 M_{J_{\text{up}}}$  exoplanet with three different initial fuzzy-core extents—mild, moderate, and extended—modeled with the AQUA EOS, against a homogeneous adiabatic Sonora-Bobcat model. The helium fraction is fixed at  $Y = 0.2735$  (CD21 EOS), and all models adopt Sonora-Bobcat atmospheric boundary conditions at  $3.16 Z_{\odot}$ . The bulk metallicity is  $Z = 0.236$ , corresponding to a heavy-element mass of  $150 M_{\oplus}$ , chosen to allow substantial mixing and to test evolutionary differences between fuzzy-core configurations. Rotation and helium rain are neglected. The top panels show the interior temperature, entropy, and heavy-element fraction profiles at 0.001, 0.5, and 5 Gyr, while the bottom panels track the evolution of effective temperature, radius, and atmospheric metallicity. All fuzzy-core models begin from nearly identical temperature profiles with central temperatures of  $\sim 10^5$  K and outer entropies of  $S \sim 9.5 k_B/\text{baryon}$  (hot-start conditions). The extended fuzzy core mixes rapidly and homogenizes, followed by the moderate case, while the mild core persists with little mixing over 10 Gyr. Relative to the homogeneous model, the fuzzy-core cases show median deviations of 8% to 12% in  $T_{\text{eff}}$  and 8% to 13% in radius. The atmospheric metallicity rises from  $Z = 0.02$  (mild) to  $Z = 0.25$  (extended).

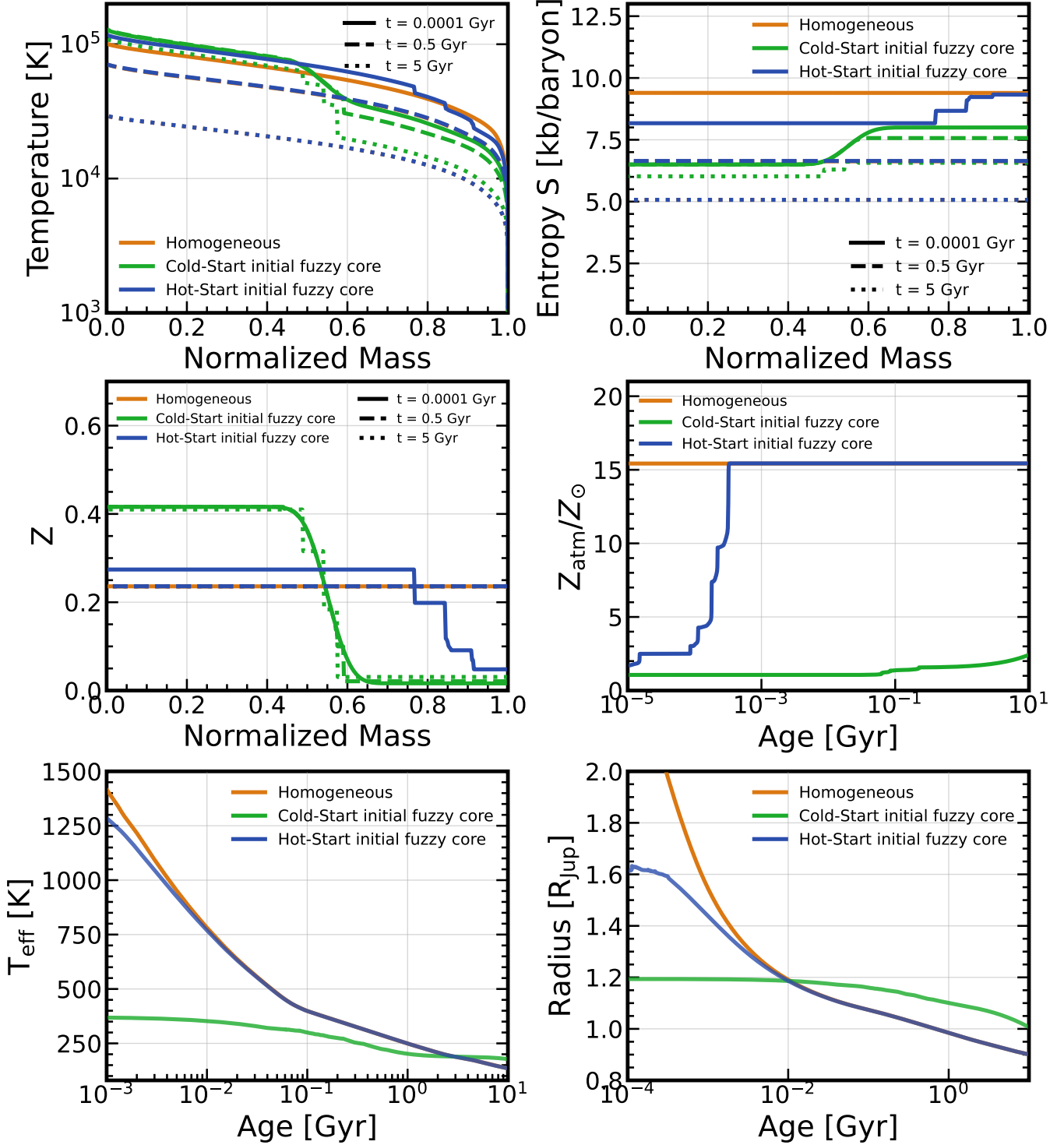


**Figure 8.** Comparison of evolutionary models for a  $2 M_{\text{Jup}}$  planet with different initial conditions: a hot-start initial fuzzy-core model (blue lines), a cold-start initial fuzzy-core model (green lines), and a homogeneous Sonora Bobcat model (orange lines). All calculations employ the Sonora Bobcat atmospheric boundary conditions at  $3.16 Z_{\odot}$ , the SCvH95 EOS for hydrogen–helium, and the AQUA EOS for heavy elements. The homogeneous model is coreless and assumes an envelope metallicity of  $Z = 0.236$ . Rotation and helium rain are neglected, and the fuzzy core distributions are the same initially. We assume the Ledoux criterion for convective stability. The initial central temperatures for the hot fuzzy core model and the cold fuzzy core model are  $1.5 \times 10^5$  K and  $1.2 \times 10^5$  K; however, their outer entropies are 9 and  $8 k_B/\text{baryon}$ , respectively. The homogeneous model starts at  $10 k_B/\text{baryon}$ . The hot-start fuzzy-core model rapidly homogenizes within  $\sim 0.1$  Myr and converges to the homogeneous track, while the cold-start model mixes more slowly, preserving its compositional gradient for over 10 Gyr. At Gyr timescales, the hot-start model shows differences of  $< 0.5$  K in  $T_{\text{eff}}$  and  $\sim 0.01\%$  in radius compared to the homogeneous case, whereas the cold-start model remains hotter by  $\sim 50$  K, with radii larger by  $\sim 13\%$  and a correspondingly hotter interior. The atmospheric metallicity also differs: rising to  $Z \sim 15 Z_{\odot}$  in the hot-start case and to  $Z \sim 2.5 Z_{\odot}$  in the cold-start case.

Bobcat atmospheric boundary conditions at  $3.16 Z_{\odot}$ , the SCvH95 EOS for hydrogen–helium, and the AQUA EOS for heavy elements. For clarity, rotation and helium rain are excluded from this comparison. The initial entropies of the cold- and hot-start fuzzy-core models are  $8 k_B/\text{baryon}$  and  $9 k_B/\text{baryon}$ , respectively, corresponding to a central temperature difference of  $\sim 30,000$  K. The homogeneous model is also initialized in a hot-start state.

The results, shown in Figure 8, highlight clear differences in both the thermal evolution and structural properties of the models. Over time, the hot-start fuzzy-core model converges to the homogeneous case, with effective temperatures differing by less than 0.5 K and radii by only  $\sim 0.01\%$  (bottom panels). In contrast, the cold-start fuzzy-core model evolves more distinctly, cooling to an effective temperature  $\sim 90$  K higher and yielding radii larger by  $\sim 13\%$  relative to the homogeneous model. The mixing histories also diverge: the hot-start fuzzy-core model homogenizes within 0.001 Gyr, erasing its initial gradient, whereas the cold-start model mixes more slowly and retains its compositional structure for up to 10 Gyr (middle left panel).

These evolutionary pathways have direct implications for atmospheric properties (see middle right panel). In the hot-start case, the envelope becomes substantially enriched, with atmospheric metallicities rising to  $Z \approx 0.23$  by 10 Gyr. In contrast, the cold-start model maintains only modest enrichment, with atmospheric metallicity reaching  $Z \approx 0.04$  over the same timescale. Together, these results underscore the sensitivity of planetary evolution to initial thermal states, showing that hot- versus cold-start conditions can imprint long-lasting signatures on both bulk properties and observable atmospheric compositions. We note that our best-fit models for Jupiter and Saturn, in which initially fuzzy cores survive to the present day, have low initial internal entropies (Sur et al. 2025a; Tejada Arevalo et al. 2025).

## 5. SAMPLE NEXT-GENERATION EVOLUTIONS OF GIANT EXOPLANETS

Early models of planet formation often assumed that all heavy elements accreted directly to the core. However, more sophisticated formation models and recent measurements of the solar-system giants now suggest that a substantial fraction—if not the majority—of accreted solids are deposited into the envelope through ablation and fragmentation once the core reaches a mass of roughly  $0.5\text{--}3 M_{\oplus}$  (Inaba & Ikoma 2003; Iaroslavitz & Podolak 2007; Hori & Ikoma 2011; Brouwers et al. 2018; Valletta & Helled 2019; Valletta & Helled 2020). Determining both the total amount of heavy elements

and their distribution within giant exoplanets remains a major challenge, as these properties are highly sensitive to the specific formation pathways (Mordasini et al. 2009; Danti et al. 2023; Mordasini et al. 2015). Detailed formation models for giant planets are currently available only for Jupiter (Lozovsky et al. 2017; Stevenson et al. 2022) and Saturn (Bodenheimer et al. 2025), and even in these cases, the origin of their fuzzy cores is still unresolved (Helled & Stevenson 2017; Helled et al. 2022; Meier et al. 2025; Fuentes et al. 2025). In this section, we assume that all planets begin with fuzzy cores; however, whether these structures survive throughout evolution depends strongly on their initial interior entropy profiles (Knierim & Helled 2024; Tejada Arevalo et al. 2025; Sur et al. 2025a) as well as their extent, as discussed in §4.7. To investigate this, we show the potential effects of both cold- and hot-start initial conditions (Spiegel & Burrows 2012), and further we compare evolutionary outcomes under the Ledoux and Schwarzschild criteria for convection as done in Sur et al. (2025b).

We compare evolutionary models for giant exoplanets that incorporate updated treatments of heavy-element distributions, updated EOSs, and new atmospheric boundary conditions against the heritage Sonora Bobcat models (Marley et al. 2021). In our updated calculations, heavy elements are treated explicitly with the AQUA EOS, hydrogen–helium is modeled with the latest CD21 EOS (Chabrier & Debras 2021), and the atmospheric boundary conditions are taken from the updated grids of Chen et al. (2023). Helium rain is also included, utilizing the hydrogen–helium miscibility curve of Lorenzen et al. (2009, 2011), shifted by +300 K, which simultaneously reproduces the observed cooling histories of Jupiter and Saturn with fuzzy cores (Sur et al. 2025a). The initial fuzzy-core configurations in this study are constructed following the recent mass–bulk metallicity relation of Chachan et al. (2025), with cold starting entropies chosen to preserve composition gradients throughout the evolution. We present representative models for total masses of 0.3, 1, 2, and  $4 M_{\text{Jup}}$ , which correspond to heavy-element masses of 21, 42, 71, and  $128 M_{\oplus}$ , respectively (Chachan et al. 2025). All models include a compact core of  $3M_{\oplus}$ , are non-rotating, and are not tuned to reproduce any particular observable, thereby providing a controlled comparison with earlier homogeneous models. For additional context, we also include Jupiter and Saturn fits from Sur et al. (2025a), which differ from the other cases in that they include rotation and are explicitly tuned to match both the thermal evolution and the low-order gravitational moments of the two planets. Therefore, our  $1 M_{\text{Jup}}$  and  $0.3 M_{\text{Jup}}$  planets presented in this work

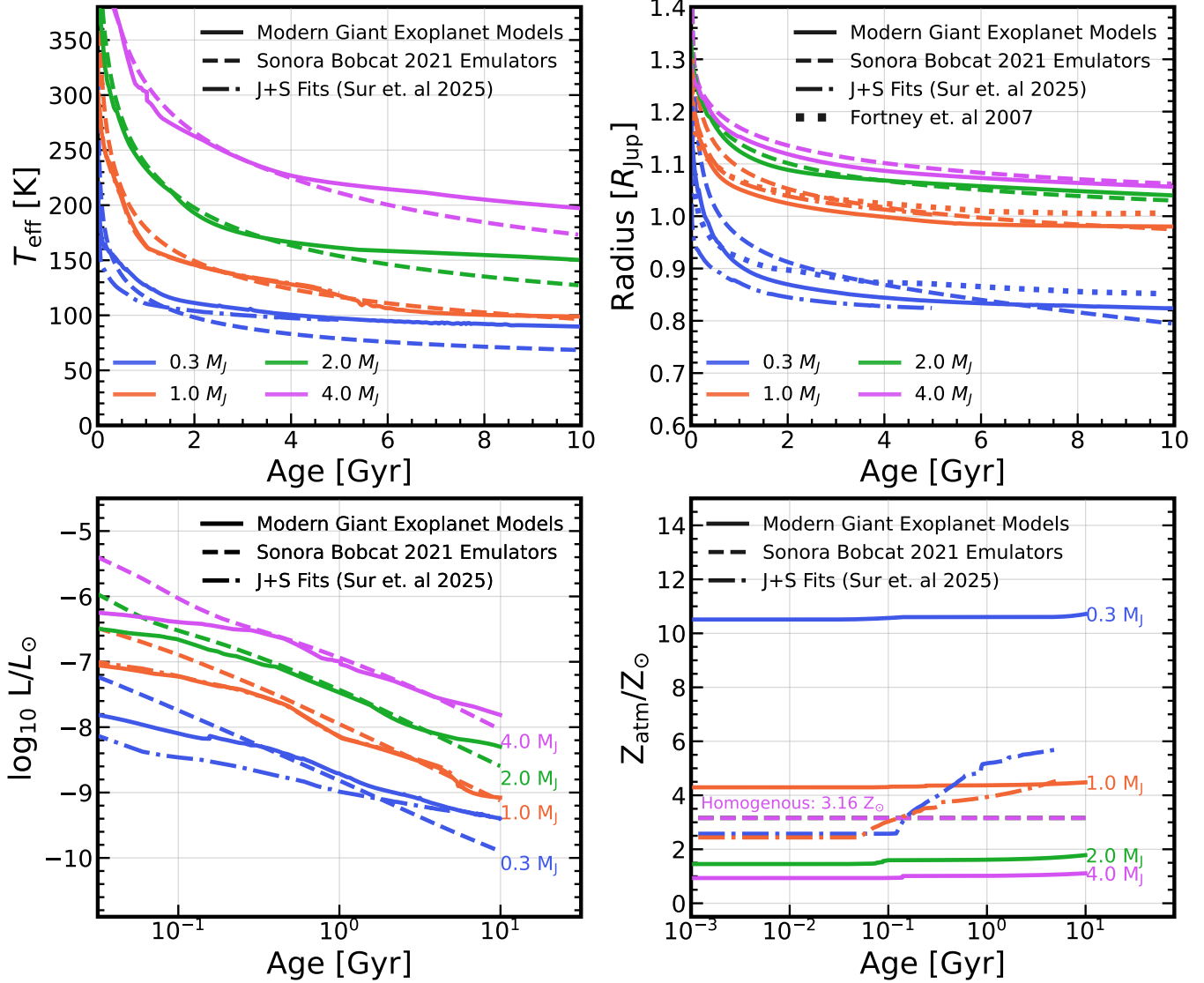


**Figure 9.** Comparison of sample next-generation evolutionary models for giant exoplanets with updated treatments of heavy-element distributions, EOS, and boundary conditions against the Sonora Bobcat heritage models. Solid lines represent models from this work, dashed lines are Sonora Bobcat emulators (Marley et al. 2021), and dash-dot lines correspond to Jupiter and Saturn fits from Sur et al. (2025a). We also show in the top-right panel, for comparison, using the dotted line, the radii for 0.3 and 1  $M_{Jup}$  giant planets from (Fortney et al. 2007), which uses a compact rocky core of  $25 M_{\oplus}$ . Our models incorporate heavy-element distributions treated with the AQUA EOS (Haldemann et al. 2020), the latest H-He EOS of CD21 (Chabrier & Debras 2021), updated atmospheric boundary conditions from Chen et al. (2023), and helium rain based on the miscibility curve of L0911 shifted by +300 K. In contrast, the Sonora models assume a homogeneous  $3.16 Z_{\odot}$  envelope, approximating heavy elements with an effective helium fraction  $Y' = Y + Z = 0.321$ . Models are shown for 0.3, 1, 2, and 4  $M_{Jup}$ , corresponding to heavy-element masses of 21, 42, 71, and  $128 M_{\oplus}$ . These initial conditions follow the bulk metallicity relation of Chachan et al. (2025), with cold entropies chosen to preserve composition gradients during the entire evolution. We use the Ledoux criterion for convective stability. All models are non-rotating and not tuned to match observables. At 5 Gyr, effective temperatures differ from the homogeneous Sonora sequences by 18, 1.8, 7.4, and 8.3 K for 0.3, 1, 2, and 4  $M_{Jup}$ , respectively, while radii differ by only  $\sim 2\%$ . The Fortney et al. (2007) models, however, predict a much higher radius by up to 5%. Luminosities agree for higher-mass planets, but the 0.3  $M_{Jup}$  model remains an order of magnitude brighter. Outer metallicities differ significantly, reflecting the influence of interior mixing and helium rain.

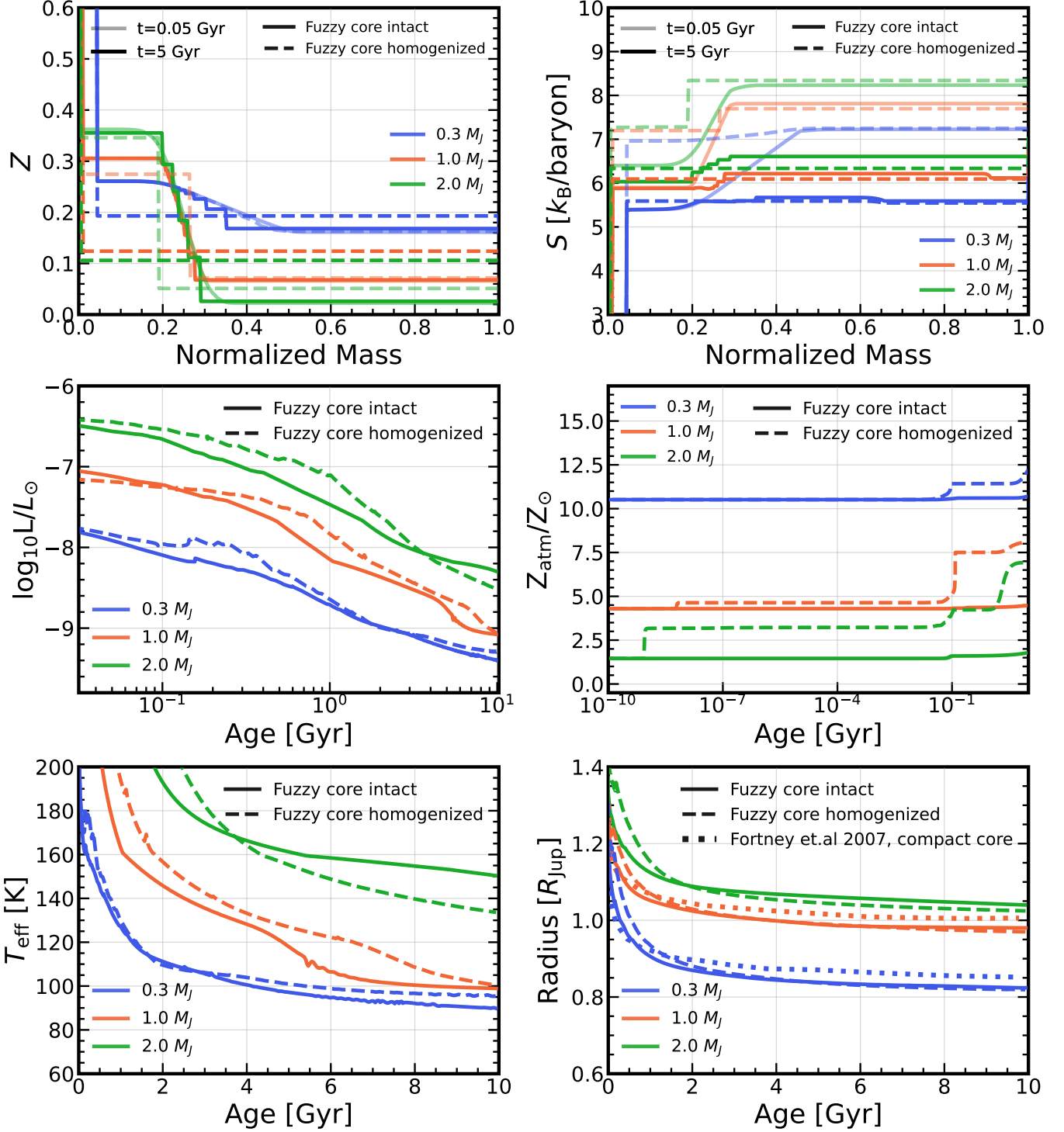


**Figure 10.** Comparison of next-generation evolutionary models in which fuzzy cores either survive (solid lines) or homogenize (dashed lines) during 10 Gyr of evolution for  $0.3 M_{J_{\text{up}}}$ ,  $1 M_{J_{\text{up}}}$ , and  $2 M_{J_{\text{up}}}$  exoplanets, incorporating the same combined updated physics as in Figure 9. All models begin with an initial fuzzy core extending to 30% of the total planetary mass, but differ in their initial entropy profiles: cold-start models (interior entropies  $\sim 6$  to  $6.5$  k<sub>B</sub>/baryon), where the fuzzy core survives throughout the evolution, versus hot-start models (interior entropies  $\sim 7.5$  to  $8.5$  k<sub>B</sub>/baryon), where the fuzzy core rapidly homogenizes. This is demonstrated in the top panels, which show  $Z$  and entropy distributions at 0.05 Gyr (translucent lines) and 5 Gyr (dark lines). The middle left panel shows the log of luminosities. In the middle right panel, atmospheric metallicities are shown to have increased by 3 to 5  $Z_{\odot}$  in models that homogenized as a result of substantial mixing. In the cases where the fuzzy core survives, the effective temperatures differ by  $-4.0$  K,  $-9.1$  K, and  $+4.8$  K, while the radii differ by 0.11%,  $-0.05\%$ , and  $+1.54\%$  for  $0.3$ ,  $1$ , and  $2 M_{J_{\text{up}}}$  planets, respectively, relative to the homogenized cases. We also compare the radii with the models of Fortney et al. (2007), which considered giant exoplanets with a compact  $25 M_{\oplus}$  core at 1 AU. Their models predict radii that are larger by 2.5 to 3.5% compared to the fuzzy-core models presented here.

are not updated evolutionary models for Jupiter and Saturn, but rather representative exoplanet analogs at those masses that incorporate all the physical upgrades discussed herein.

Our emulated comparison Sonora Bobcat models assume a homogeneous  $3.16 Z_{\odot}$  envelope, where the influence of heavy elements is not modeled with a dedicated EOS, but is instead approximated by adopting an effective helium fraction  $Y' = Y + Z = 0.3219$  as in [Marley et al. \(2021\)](#), uniformly distributed in the envelope. Neither helium rain nor the evolution of an initial fuzzy core are considered for the Sonora models. This distinction highlights a key difference: while the heritage models capture bulk metallicity in an approximate way and assume homogeneity in the envelope, our calculations account for the radial distribution of heavy elements and their impact on planetary structure and cooling. The goal of this overall exercise is to demonstrate the differences between heritage evolutionary models now used widely and more sophisticated models, however provisional.

The results, shown in Figure 9, reveal systematic differences between the homogeneous (dashed lines) and fuzzy core models (solid lines). At 5 Gyr, the effective temperature offsets relative to the Sonora Bobcat sequences are 18, 1.8, 7.4, and 8.3 K for the 0.3, 1, 2, and  $4 M_{\text{Jup}}$  planets, respectively, while the radii differ by only  $\sim 1\%$ . Thus, the effect of more realistic interior structures is subtle in radius, but more noticeable in cooling rates, particularly at low masses. The lower panels of Figure 9 show that luminosities are nearly identical for the higher-mass planets (except at very late times), but the  $0.3 M_{\text{Jup}}$  case is up to an order of magnitude brighter than its homogeneous counterpart, underscoring the sensitivity of lower-mass planets to heavy-element distribution and helium rain. The outer envelope metallicities also diverge significantly with time, reflecting the role of interior mixing and the redistribution of heavy elements. Collectively, these results demonstrate that incorporating realistic micro-physics and heavy-element distributions produces modest changes at Jupiter mass and above, but can substantially alter the evolutionary trajectories of low-mass giant planets.

Next, we compare models in which the fuzzy core survives during 10 Gyr of evolution to those in which it rapidly homogenizes for planets of mass 0.3, 1, and  $2 M_{\text{Jup}}$ . All models begin with an initially extended fuzzy core encompassing roughly 30% of the total planetary mass, but differ in their initial entropy profiles. Cold-start configurations, with interior entropies of  $\sim 6\text{--}7 k_{\text{B}}/\text{baryon}$ , maintain their compositional gradients

and evolve with stable fuzzy cores, whereas hot-start models, with entropies of  $\sim 8\text{--}8.5 k_{\text{B}}/\text{baryon}$ , experience vigorous mixing that erases the gradient and produces nearly homogeneous interiors. The luminosity evolution for all three masses is shown in the top-left panel, while the top-right panel highlights the evolution of atmospheric metallicities, which increase substantially, by approximately  $3\text{--}5 Z_{\odot}$ —in the homogenized models as a result of enhanced convective mixing. The middle panels of Figure 10 illustrate this evolution through the heavy-element mass fraction and entropy distributions at 0.05 Gyr (translucent lines) and 5 Gyr (dark lines), showing the rapid homogenization in the hot-start cases.

Quantitatively, the cold-start models with surviving fuzzy cores exhibit modest differences in their thermal and structural properties compared to the homogenized cases. At 5 Gyr, their effective temperatures differ by  $-4.0$  K,  $-9.1$  K, and  $+4.8$  K, while the corresponding radii differ by 0.11%,  $-0.05\%$ , and  $+1.54\%$  for the 0.3, 1, and  $2 M_{\text{Jup}}$  planets, respectively. For additional context, we compare these results to the compact-core models of [Fortney et al. \(2007\)](#), who considered giant planets with a  $25 M_{\oplus}$  solid core at 1 AU. Their models predict radii larger by 2.5–3.5% relative to our fuzzy-core models, indicating that extended heavy-element distributions produce slightly more compact structures, but are also sensitive to the bulk metallicities. Overall, these results demonstrate that the survival or erosion of fuzzy cores introduces measurable, but subtle, differences in planetary cooling histories, while strongly influencing atmospheric metallicities—a potentially observable diagnostic of interior mixing and formation history ([Knierim & Helled 2024, 2025](#)).

Finally, the choice of convection criterion also introduces systematic, but measurable, differences in planetary evolution as shown in Figure 11. For both the  $0.3 M_{\text{Jup}}$  and  $1 M_{\text{Jup}}$  cases, models using the Schwarzschild criterion evolve to slightly hotter tracks than those adopting the Ledoux criterion, with effective temperatures higher by about 5–10 K at Gyr ages. The radius response is comparatively modest, shrinking by only  $\sim 0.1\%$ . More importantly, the treatment of convection affects the efficiency of mixing: the Schwarzschild criterion permits greater redistribution of heavy elements within the envelope, leading to a noticeable increase in atmospheric metallicity over time. This effect is especially pronounced in the  $1 M_{\text{Jup}}$  case, where enhanced mixing drives surface abundances to significantly higher values than in the Ledoux models.

The onset of helium rain further accentuates the differences between the two convection criteria. In Ledoux models, the compositional gradient produced by helium

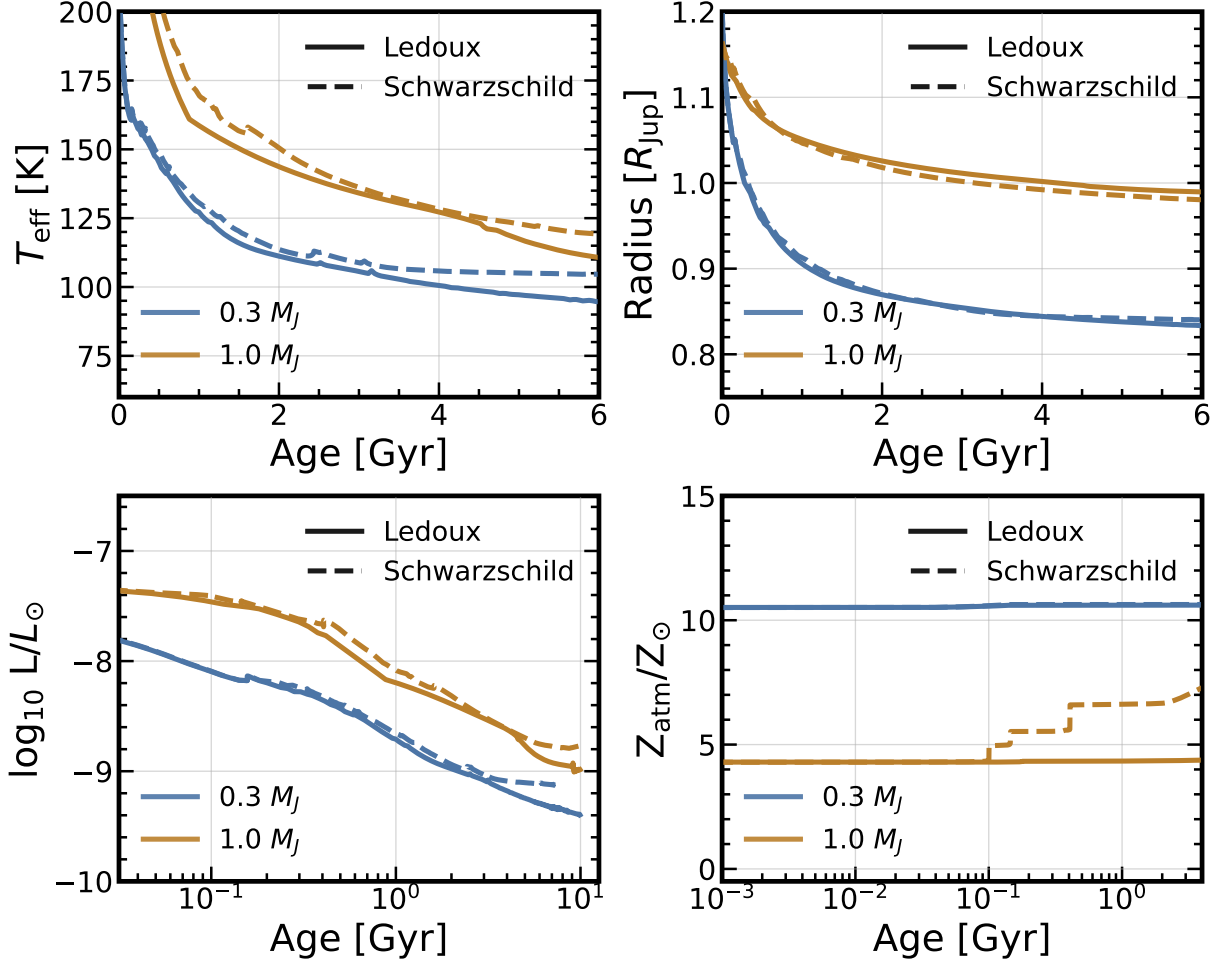


**Figure 11.** Comparison of evolutionary models using the Ledoux (solid lines) and Schwarzschild (dashed lines) convection criteria for  $0.3 M_{\text{Jup}}$  and  $1 M_{\text{Jup}}$  exoplanets, incorporating the combined updated physics. All models begin with an initial fuzzy core extending to 30% of the normalized planetary mass and include heavy elements treated with the AQUA EOS, hydrogen–helium with the CD21 EOS, atmospheric boundary conditions from Chen et al. (2023), and helium rain based on the miscibility curve of L0911 shifted by +300 K. Relative to the Ledoux cases, the Schwarzschild models evolve to slightly higher effective temperatures—hotter by about 5–10 K—while showing negligible differences in radius. The onset of helium rain produces a marked divergence between the two convection treatments: in Ledoux models, helium rain stabilizes the interior and suppresses convection, leading to cooler  $T_{\text{eff}}$  tracks, whereas in Schwarzschild models, the absence of compositional stabilization allows continued mixing and a transient increase in effective temperature after helium rain. The Schwarzschild criterion also enables more efficient redistribution of heavy elements, resulting in higher atmospheric metallicities, particularly for the  $1 M_{\text{Jup}}$  planet, where the atmosphere is enriched by approximately  $3 Z_{\odot}$ .

phase separation stabilizes the fluid against convection, reducing the efficiency of heat transport and leading to a drop in effective temperature. By contrast, the Schwarzschild models—insensitive to composition gradients—allow convection to persist even during helium rain, which facilitates more efficient energy release from the interior and temporarily raises  $T_{\text{eff}}$ . As a result, the two treatments yield divergent thermal histories and surface compositions, despite their nearly identical global radii. These results highlight that, while structural differences may appear small, the choice of convection criterion plays a critical role in controlling how

helium rain and internal mixing shape the observable properties of giant planets.

## 6. CONCLUSION

In this paper, we compared old models of giant exoplanets with new models incorporating the latest physical insights, as determined from detailed modeling of Jupiter and Saturn. These new aspects include new equations of state, helium rain, “fuzzy” extended heavy-element cores, stably-stratified regions, and inhomogeneous heavy-element distributions in the envelope. Also included are new atmosphere boundary conditions which

factor in ammonia clouds. First, we isolated the differences between old and new models for each new feature individually. Then, we combined the new features into representative baseline models and determined the overall differences in model observables and in the interiors of all new features collectively. To make these comparisons, we created emulators of these past models using our new code **APPLE**. What we found were important variations between old and new which should be addressed in the next generation of giant exoplanet models. We also found that the initial thermal profiles, particularly in the interiors, can have important effects on the temporal evolution of observables, such as effective temperature and atmospheric metallicity. We focused on the planet mass range from 0.3 to 4.0 M<sub>J</sub>.

Our study is meant to highlight the need for a new generation of giant exoplanet evolutionary models, but we did not in this paper provide such a new model suite and are deferring that task to later work. We also note that the potential effects of semiconvection were not explicitly addressed, though we did contrast models using the Ledoux and Schwarzschild convective criteria. The latter is in the limit of very efficient doubly-diffusive mixing, while the former mutes it completely and allows negative composition gradients to be stabilizing. We find that whether helium rain in the lower-mass giants heats or cools their atmospheres hinges upon which limit obtains.

Our simulations have limitations. Foremost is the ongoing need for consistent equations of state for ternary

mixtures. We have been forced to use the additive volume law. In addition, databases in the literature for individual constituents are thermodynamically consistent only to percents (Tejada Arevalo et al. 2024). Also, in this study we did not include the effects of rotation. Rotation can affect the size and evolution of the convective envelope and the character of convection (Fuentes et al. 2023, 2024). Moreover, we need a better model for hydrogen/helium miscibility and the dynamics and extent of the helium rain region. Finally, as noted, the potential role of semiconvection in thermal and material transport (Leconte & Chabrier 2012; Polman & Mordasini 2024) is not yet well understood. Nevertheless, we have demonstrated that heritage evolutionary models of giant exoplanets since the early work of Burrows et al. (1995), which assumed among other things, homogeneity and adiabaticity, are in need of retooling so that what emerges can play a productive role in the emerging era of precision exoplanetary science.

## ACKNOWLEDGMENTS

Funding for this research was provided by the Center for Matter at Atomic Pressures (CMAP), a National Science Foundation (NSF) Physics Frontier Center, under Award PHY-2020249. Any opinions, findings, conclusions, or recommendations expressed in this material are those of the author(s) and do not necessarily reflect those of the National Science Foundation.

## REFERENCES

Aguichine, A., Batalha, N., Fortney, J. J., et al. 2025, preprint, 1. <https://arxiv.org/abs/2412.17945v2>

Arras, P., & Bildsten, L. 2006, ApJ, 650, 394, doi: [10.1086/506011](https://doi.org/10.1086/506011)

Baraffe, I., Chabrier, G., Allard, F., & Hauschildt, P. H. 1998, A&A, 337, 403. <https://articles.adsabs.harvard.edu/pdf/1998A%26A...337..403B>

Baraffe, I., Chabrier, G., Barman, T. S., Allard, F., & Hauschildt, P. H. 2003, Astronomy and Astrophysics, 402, 701, doi: [10.1051/0004-6361:20030252](https://doi.org/10.1051/0004-6361:20030252)

Bodenheimer, P. 1976, Icarus, 29, 165, doi: [10.1016/0019-1035\(76\)90042-7](https://doi.org/10.1016/0019-1035(76)90042-7)

Bodenheimer, P., & Pollack, J. B. 1986, Icarus, 67, 391, doi: [10.1016/0019-1035\(86\)90122-3](https://doi.org/10.1016/0019-1035(86)90122-3)

Bodenheimer, P., Stevenson, D. J., Lissauer, J. J., & D'Angelo, G. 2025, PSJ, 6, 143, doi: [10.3847/PSJ/add0b](https://doi.org/10.3847/PSJ/add0b)

Bolton, S. J., Lunine, J., Stevenson, D., et al. 2017, Space Science Reviews, 213, 5, doi: [10.1007/s11214-017-0429-6](https://doi.org/10.1007/s11214-017-0429-6)

Brouwers, M. G., Vazan, A., & Ormel, C. W. 2018, A&A, 611, A65, doi: [10.1051/0004-6361/201731824](https://doi.org/10.1051/0004-6361/201731824)

Burrows, A., Hubbard, W. B., Lunine, J. I., & Liebert, J. 2001, Reviews of Modern Physics, 73. <https://journals.aps.org/rmp/pdf/10.1103/RevModPhys.73.719>

Burrows, A., Hubbard, W. B., Saumon, D., & Lunine, J. I. 1993, ApJ, 406, 158, doi: [10.1086/172427](https://doi.org/10.1086/172427)

Burrows, A., Saumon, D., Guillot, T., Hubbard, W., & Luninet, J. I. 1995, Letters to Nature, 375, 299. <https://www.nature.com/articles/375299a0>

Burrows, A., Marley, M., Hubbard, W., et al. 1997, ApJ, 491, 856. <https://iopscience.iop.org/article/10.1086/305002/pdf>

Chabrier, G. 2003, Publications of the Astronomical Society of the Pacific, 115, 763, doi: [10.1086/376392](https://doi.org/10.1086/376392)

Chabrier, G., & Baraffe, I. 1997, A&A, 327, 1039. <https://articles.adsabs.harvard.edu/pdf/1997A%26A...327.1039C>

Chabrier, G., & Debras, F. 2021, *ApJ*, 917, 6pp, doi: [10.3847/1538-4357/abfc48](https://doi.org/10.3847/1538-4357/abfc48)

Chabrier, G., Mazevert, S., & Soubiran, F. 2019, *ApJ*, 872, 27pp, doi: [10.3847/1538-4357/aaf99f](https://doi.org/10.3847/1538-4357/aaf99f)

Chachan, Y., Fortney, J. J., Ohno, K., Thorngren, D., & Murray-Clay, R. 2025, arXiv e-prints, arXiv:2509.20428, doi: [10.48550/arXiv.2509.20428](https://doi.org/10.48550/arXiv.2509.20428)

Chen, Y.-X., Burrows, A., Sur, A., & Arevalo, R. T. 2023, *ApJ*, 957, 8, doi: [10.3847/1538-4357/acf456](https://doi.org/10.3847/1538-4357/acf456)

Danti, C., Bitsch, B., & Mah, J. 2023, *A&A*, 679, L7, doi: [10.1051/0004-6361/202347501](https://doi.org/10.1051/0004-6361/202347501)

Debras, F., & Chabrier, G. 2019, *ApJ*, 872, 22pp, doi: [10.3847/1538-4357/aaff65](https://doi.org/10.3847/1538-4357/aaff65)

Demarcus, W. C. 1958, *AJ*, 63, 2, doi: [10.1086/107672](https://doi.org/10.1086/107672)

Fortney, J. J., & Hubbard, W. B. 2003, *Icarus*, 164, 228, doi: [10.1016/S0019-1035\(03\)00130-1](https://doi.org/10.1016/S0019-1035(03)00130-1)

—. 2004, *ApJ*, 608, 1039, doi: [10.1086/420765](https://doi.org/10.1086/420765)

Fortney, J. J., Ikoma, M., Nettelmann, N., Guillot, T., & Marley, M. S. 2011, *The Astrophysical Journal*, 729, 32, doi: [10.1088/0004-637X/729/1/32](https://doi.org/10.1088/0004-637X/729/1/32)

Fortney, J. J., Marley, M. S., & Barnes, J. W. 2007, *ApJ*, 659, 1661, doi: [10.1086/512120](https://doi.org/10.1086/512120)

Fuentes, J. R., Anders, E. H., Cumming, A., & Hindman, B. W. 2023, *ApJ* Preprint, 18, <https://arxiv.org/pdf/2305.09921.pdf>

Fuentes, J. R., & Cumming, A. 2021, *Physical Review Fluids*, 5, 124501, doi: [10.1103/PhysRevFluids.5.124501](https://doi.org/10.1103/PhysRevFluids.5.124501)

Fuentes, J. R., Hindman, B. W., Fraser, A. E., & Anders, E. H. 2024, preprint

Fuentes, J. R., Mankovich, C. R., & Sur, A. 2025, *ApJL*, 988, L49, doi: [10.3847/2041-8213/adef0a](https://doi.org/10.3847/2041-8213/adef0a)

Graboske, H. C., Pollack, J. B., Grossman, A. S., & Olnessi, R. J. 1975, *The Astrophysical Journal*, 199, 265. <https://articles.adsabs.harvard.edu/pdf/1975ApJ...199.265G>

Grossman, A. S., Graboske, H., Pollack, J., Reynolds, R., & Summers, A. 1972, *Physics of the Earth and Planetary Interiors*, 6, 91, doi: [10.1016/0031-9201\(72\)90038-6](https://doi.org/10.1016/0031-9201(72)90038-6)

Guillot, T., Chabrier, G., Gautier, D., & Morel, P. 1995, *ApJ*, 11, 1. <https://articles.adsabs.harvard.edu/pdf/1995ApJ...450.463G>

Haldemann, J., Alibert, Y., Mordasini, C., & Benz, W. 2020, *Astrophysics A&A*, 643, 105, doi: [10.1051/0004-6361/202038367](https://doi.org/10.1051/0004-6361/202038367)

Helled, R., & Stevenson, D. 2017, *The Astrophysical Journal Letters*, 840, L4, doi: [10.3847/2041-8213/aa6d08](https://doi.org/10.3847/2041-8213/aa6d08)

Helled, R., & Stevenson, D. 2017, *ApJL*, 840, L4, doi: [10.3847/2041-8213/aa6d08](https://doi.org/10.3847/2041-8213/aa6d08)

Helled, R., Stevenson, D. J., Lunine, J. I., et al. 2022, *Icarus*, 378, 114937, doi: [10.1016/j.icarus.2022.114937](https://doi.org/10.1016/j.icarus.2022.114937)

Hori, Y., & Ikoma, M. 2011, *MNRAS*, 416, 1419, doi: [10.1111/j.1365-2966.2011.19140.x](https://doi.org/10.1111/j.1365-2966.2011.19140.x)

Howard, S., & Guillot, T. 2023, *A&A*, 672, doi: [10.5281/zenodo](https://doi.org/10.5281/zenodo)

Howard, S., Helled, R., & Müller, S. 2025, *A&A*, 693, L7, doi: [10.1051/0004-6361/202452783](https://doi.org/10.1051/0004-6361/202452783)

Howard, S., Müller, S., & Helled, R. 2024, preprint, 1. <https://arxiv.org/abs/2407.11120>

Howard, S., Guillot, T., Bazot, M., et al. 2023, *A&A*, doi: [10.5281/zenodo.7598377](https://doi.org/10.5281/zenodo.7598377)

Hubbard, W. 1970, *ApJ*, 162. <https://articles.adsabs.harvard.edu/pdf/1970ApJ...162..687H>

Hubbard, W. B. 1966, *ApJ*, 146, 858, doi: [10.1086/148961](https://doi.org/10.1086/148961)

Hubbard, W. B. 1968, *The Astrophysical Journal*, 152. <https://articles.adsabs.harvard.edu/pdf/1968ApJ...152..745H>

Hubbard, W. B. 1969, *ApJ*, 155, 333, doi: [10.1086/149868](https://doi.org/10.1086/149868)

Hubbard, W. B. 1977, *Icarus*, 30, 305, doi: [10.1016/0019-1035\(77\)90164-6](https://doi.org/10.1016/0019-1035(77)90164-6)

Hubbard, W. B., & Smoluchowski, R. 1973, *SSRv*, 14, 599, doi: [10.1007/BF00166644](https://doi.org/10.1007/BF00166644)

Iaroslavitz, E., & Podolak, M. 2007, *Icarus*, 187, 600, doi: [10.1016/j.icarus.2006.10.008](https://doi.org/10.1016/j.icarus.2006.10.008)

Iess, L., Militzer, B., Kaspi, Y., et al. 2019, *Science*, 364, doi: [10.1126/science.aat2965](https://doi.org/10.1126/science.aat2965)

Inaba, S., & Ikoma, M. 2003, *A&A*, 410, 711, doi: [10.1051/0004-6361:20031248](https://doi.org/10.1051/0004-6361:20031248)

Knierim, H., & Helled, R. 2024, *ApJ*, 227, 13. <https://arxiv.org/abs/2407.09341>

—. 2025, *A&A*, 698, 1. <https://arxiv.org/abs/2504.12118>

Knierim, H., Shibata, S., & Helled, R. 2022, *A&A*, 665, L5, doi: [10.1051/0004-6361/202244516](https://doi.org/10.1051/0004-6361/202244516)

Leconte, J., & Chabrier, G. 2012, *A&A*, 540, 20, doi: [10.1051/0004-6361/201117595](https://doi.org/10.1051/0004-6361/201117595)

Ledoux, P. 1947, *ApJ*, 105

Lissauer, J. J. 1987, *Icarus*, 69, 249, doi: [10.1016/0019-1035\(87\)90104-7](https://doi.org/10.1016/0019-1035(87)90104-7)

Liu, L., Li, Z.-G., Chen, Q.-F., et al. 2025, *PhRvB*, 112, 064111, doi: [10.1103/69y2-p18x](https://doi.org/10.1103/69y2-p18x)

Lorenzen, W., Holst, B., & Redmer, R. 2009, *Physical Review Letters*, 102, doi: [10.1103/PhysRevLett.102.115701](https://doi.org/10.1103/PhysRevLett.102.115701)

—. 2011, *Physical Review B*, 84, doi: [10.1103/PhysRevB.84.235109](https://doi.org/10.1103/PhysRevB.84.235109)

Lozovsky, M., Helled, R., Rosenberg, E. D., & Bodenheimer, P. 2017, *ApJ*, 836, 227, doi: [10.3847/1538-4357/836/2/227](https://doi.org/10.3847/1538-4357/836/2/227)

Mankovich, C., Fortney, J. J., & Moore, K. L. 2016, *ApJ*, 832, 13pp, doi: [10.3847/0004-637X/832/2/113](https://doi.org/10.3847/0004-637X/832/2/113)

Mankovich, C. R., & Fortney, J. J. 2020, *The Astrophysical Journal*, 889, 51, doi: [10.3847/1538-4357/ab6210](https://doi.org/10.3847/1538-4357/ab6210)

Mankovich, C. R., & Fuller, J. 2021, *Nature Astronomy*, 5, 1103, doi: [10.1038/s41550-021-01448-3](https://doi.org/10.1038/s41550-021-01448-3)

Marley, M. S., Saumon, D., Visscher, C., et al. 2021, *The Astrophysical Journal*, 920, 85, doi: [10.3847/1538-4357/ac141d](https://doi.org/10.3847/1538-4357/ac141d)

Mazevet, S., Licari, A., Chabrier, G., & Potekhin, A. Y. 2019, *Astronomy and Astrophysics*, 621, 1, doi: [10.1051/0004-6361/201833963](https://doi.org/10.1051/0004-6361/201833963)

—. 2021, *Astronomy and Astrophysics*, 621, 1, doi: [10.1051/0004-6361/201833963](https://doi.org/10.1051/0004-6361/201833963)

Meier, T., Reinhardt, C., Shibata, S., et al. 2025, preprint, doi: [10.3847/1538-4357/addbe6](https://doi.org/10.3847/1538-4357/addbe6)

Miguel, Y., Guillot, T., & Fayon, L. 2016, *A&A*, 596, doi: [10.1051/0004-6361/201629732](https://doi.org/10.1051/0004-6361/201629732)

Militzer, B., & Hubbard, W. B. 2013, *The Astrophysical Journal*, 774, 148, doi: [10.1088/0004-637X/774/2/148](https://doi.org/10.1088/0004-637X/774/2/148)

—. 2024, *Icarus*, 411, 115955, doi: [10.1016/j.icarus.2024.115955](https://doi.org/10.1016/j.icarus.2024.115955)

Militzer, B., Hubbard, W. B., Wahl, S., et al. 2022, *The Planetary Science Journal*, 3, 185, doi: [10.3847/PSJ/ac7ec8](https://doi.org/10.3847/PSJ/ac7ec8)

Mizuno, H. 1980, *Progress of Theoretical Physics*, 64, 544, doi: [10.1143/PTP.64.544](https://doi.org/10.1143/PTP.64.544)

Mordasini, C., Alibert, Y., & Benz, W. 2009, *A&A*, 501, 1139, doi: [10.1051/0004-6361/200810301](https://doi.org/10.1051/0004-6361/200810301)

Mordasini, C., Mollière, P., Dittkrist, K. M., Jin, S., & Alibert, Y. 2015, *International Journal of Astrobiology*, 14, 201, doi: [10.1017/S1473550414000263](https://doi.org/10.1017/S1473550414000263)

Müller, S., Helled, R., & Cumming, A. 2020, *A&A*, 638, doi: [10.1051/0004-6361/201937376](https://doi.org/10.1051/0004-6361/201937376)

Peebles, P. J. E. 1964, *The Astrophysical Journal*, 140, 328, doi: [10.1086/147922](https://doi.org/10.1086/147922)

Phillips, M. W., Tremblin, P., Baraffe, I., et al. 2020, *A&A*, 637, A38, doi: [10.1051/0004-6361/201937381](https://doi.org/10.1051/0004-6361/201937381)

Pollack, J., Hubickyj, O., Bodenheimer, P., et al. 1996, *Surface Science*, 124, 62, doi: [10.1016/j.susc.2010.03.028](https://doi.org/10.1016/j.susc.2010.03.028)

Polman, J., & Mordasini, C. 2024, *A&A*, 202, 1

Püstow, R., Nettelmann, N., Lorenzen, W., & Redmer, R. 2016, *Icarus*, 267, 323, doi: [10.1016/j.icarus.2015.12.009](https://doi.org/10.1016/j.icarus.2015.12.009)

Saumon, D., Chabrier, G., & Van Horn, H. M. 1995, *The Astrophysical Journal Supplement Series*, 99, 713

Saumon, D., & Marley, M. S. 2008, *ApJ*, 689, 1327, doi: [10.1086/592734](https://doi.org/10.1086/592734)

Schwarzchild, M., & Härm, R. 1965, *ApJ*. <http://articles.adsabs.harvard.edu/pdf/1965ApJ...142..855S>

Spiegel, D. S., & Burrows, A. 2012, *The Astrophysical Journal*, 745, 174, doi: [10.1088/0004-637X/745/2/174](https://doi.org/10.1088/0004-637X/745/2/174)

Spilker, L. 2019, *Science*, 364, 1046, doi: [10.1126/science.aat3760](https://doi.org/10.1126/science.aat3760)

Stevenson, D. J. 1982, *Planetary and Space Science*, 30, 755, doi: [10.1016/0032-0633\(82\)90108-8](https://doi.org/10.1016/0032-0633(82)90108-8)

Stevenson, D. J., Bodenheimer, P., Lissauer, J. J., & Angelo, G. D. . 2022, *The Planetary Science Journal*, 3, 15pp, doi: [10.3847/PSJ/ac5c44](https://doi.org/10.3847/PSJ/ac5c44)

Stevenson, D. J., & Salpeter, E. E. 1977, *The Astrophysical Journal Supplement Series*, 35, 221. <https://doi.org/10.1086/190479>

Sur, A., Arevalo, R. T., Su, Y., & Burrows, A. 2025a, *The Astrophysical Journal Letters*, 980, 0, doi: [10.3847/2041-8213/adad62](https://doi.org/10.3847/2041-8213/adad62)

Sur, A., Burrows, A., & Tejada Arevalo, R. 2025b. <http://arxiv.org/abs/2506.19041>

Sur, A., Su, Y., Arevalo, R. T., Chen, Y.-X., & Burrows, A. 2024, *The Astrophysical Journal*, 971, 104, doi: [10.3847/1538-4357/ad57c3](https://doi.org/10.3847/1538-4357/ad57c3)

Tejada Arevalo, R. 2025, *The Astrophysical Journal Letters*, 989, 15, doi: [10.3847/2041-8213/ad3a5](https://doi.org/10.3847/2041-8213/ad3a5)

Tejada Arevalo, R., Su, Y., Sur, A., & Burrows, A. 2024, *The Astrophysical Journal Supplement Series*, 274, 34, doi: [10.3847/1538-4365/ad6cd7](https://doi.org/10.3847/1538-4365/ad6cd7)

Tejada Arevalo, R., Sur, A., Su, Y., & Burrows, A. 2025, *The Astrophysical Journal*, 979, 0, doi: [10.3847/1538-4357/ada030](https://doi.org/10.3847/1538-4357/ada030)

Valletta, C., & Helled, R. 2019, *ApJ*, 871, 127, doi: [10.3847/1538-4357/aaf427](https://doi.org/10.3847/1538-4357/aaf427)

Valletta, C., & Helled, R. 2020, *The Astrophysical Journal*, 900, 133, doi: [10.3847/1538-4357/aba904](https://doi.org/10.3847/1538-4357/aba904)

Vazan, A., Helled, R., & Guillot, T. 2018, *A&A*, 610, 14, doi: [10.1051/0004-6361/201732522](https://doi.org/10.1051/0004-6361/201732522)

Wahl, S. M., Hubbard, W. B., Militzer, B., et al. 2017, *Geophysical Research Letters*, 44, 4649, doi: [10.1002/2017GL073160](https://doi.org/10.1002/2017GL073160)

Zapolsky, H. S., & Salpeter, E. E. 1969, *ApJ*, 158, 809, doi: [10.1086/150240](https://doi.org/10.1086/150240)